

## MIT Open Access Articles

*Diagenetic and Detrital Origin of Moretane Anomalies through the Permian-Triassic Boundary*

The MIT Faculty has made this article openly available. **Please share** how this access benefits you. Your story matters.

**Citation:** French, Katherine L. et al. "Diagenetic and Detrital Origin of Moretane Anomalies Through the Permian-Triassic Boundary." *Geochimica et Cosmochimica Acta* 84 (2012): 104-125. Web. © 2012 Elsevier B.V.

**As Published:** <http://dx.doi.org/10.1016/j.gca.2012.01.004>

**Publisher:** Elsevier Ltd.

**Persistent URL:** <http://hdl.handle.net/1721.1/70930>

**Version:** Final published version: final published article, as it appeared in a journal, conference proceedings, or other formally published context

**Terms of Use:** Article is made available in accordance with the publisher's policy and may be subject to US copyright law. Please refer to the publisher's site for terms of use.



## Diagenetic and detrital origin of moretane anomalies through the Permian–Triassic boundary

Katherine L. French<sup>a</sup>, Nicholas J. Tosca<sup>b</sup>, Changqun Cao<sup>c</sup>, Roger E. Summons<sup>d,\*</sup>

<sup>a</sup> Joint Program in Chemical Oceanography, Massachusetts Institute of Technology and Woods Hole Oceanographic Institution, Cambridge, MA 02139, United States

<sup>b</sup> Department of Earth Sciences, University of St. Andrews, St. Andrews, KY16 9AL Scotland, UK

<sup>c</sup> State Key Laboratory of Palaeobiology and Stratigraphy, Nanjing Institute of Geology and Palaeontology, Chinese Academy of Sciences, Nanjing, Jiangsu 210008, China

<sup>d</sup> Department of Earth, Atmospheric, and Planetary Sciences, Massachusetts Institute of Technology, Cambridge, MA 02139, United States

Received 20 August 2011; accepted in revised form 11 January 2012; available online 28 January 2012

### Abstract

Many biogeochemical anomalies coincide with the Late Permian Extinction (LPE; 252.28 Ma). Several mechanisms have been proposed to explain the moretane/hopane anomaly that has been identified in samples from Meishan GSSP section in southeastern China. Here, we report homohopane, 2 $\alpha$ - and 3 $\beta$ -methylhomohopane and lithological data for a drill core from the Meishan section in southeastern China. Three intervals of elevated C<sub>30</sub> moretane/hopane ratios are recorded in the Lungtan, Yinkeng and Helongshan Formations. Moretane/hopane ratios of C<sub>31–34</sub> homohopanes and the 2 $\alpha$ - and 3 $\beta$ -methylhomohopanes display the same stratigraphic patterns as the C<sub>30</sub> moretane/hopane record. In light of the multiple and parallel moretane anomalies for the homohopane and 2 $\alpha$ - and 3 $\beta$ -methylhomohopane series, enhanced input from higher plant organic matter, such as coal and peat, does not adequately explain the observed isomer patterns. Correlation of high moretane/hopane ratios with low C<sub>35</sub> Homohopane Index (HHI) and high hopane/sterane values suggest increased input of hopanoids from oxic soils. Additionally, moretane/hopane ratios show excellent correlations with total clay percentages and specific clay types, particularly chlorite, illite, and mixed layer illite/smectite. We conclude that a combination of episodic hopanoid input from soil bacteria and diagenetic effects related to redox and detrital clays generated the unique moretane/hopane patterns at Meishan.

Similar relationships of Ts/(Ts + Tm) with redox, source indicators, and lithology indicate that Ts/(Ts + Tm) is affected by the same factors controlling the moretane/hopane ratios. Berthierine, a clay that requires reducing conditions for formation, was detected in samples from the Lungtan Formation. We are unable to determine from our results whether the berthierine is authigenic or detrital, but future determination of the origin of berthierine at Meishan may offer additional environmental insight. No link between diasteranes and lithology was observed in this study suggesting that diasteranes are relatively unaffected by the detrital clay component of the Meishan sediments. In total, the results point toward the complex role of source input, lithology, and depositional redox conditions in the transformation of organic matter during maturation. Future work is required to elucidate the lithological effects on diagenetic processes, including biomarker genesis isomerization, and thermal degradation.

© 2012 Elsevier Ltd. All rights reserved.

\* Corresponding author.

E-mail address: [rsummons@mit.edu](mailto:rsummons@mit.edu) (R.E. Summons).

## 1. INTRODUCTION

Through the course of Earth's 4.5 billion year history, there have been five mass extinction events in which at least 75% of species became extinct in a geologically short time interval. Given the rapid loss of biodiversity over the past centuries, some researchers have suggested that Earth may currently be entering its sixth mass extinction (Barnosky et al., 2011). Humans are suspected to have a role in today's loss of biodiversity, but other conditions and series of events must have caused the previous five mass extinctions. The Late Permian Extinction (LPE; 252.28 Ma) (Shen et al., 2011a), which occurred shortly before the biostratigraphic Permian Triassic Boundary (PTB) as defined by the first appearance of *Hindeodus parvus*, marks the greatest loss of biodiversity in Earth history with over 90% of marine species becoming extinct (Raup, 1979; Mundil et al., 2001, 2004; Sepkoski, 2002; Erwin, 2006; Metcalfe and Isozaki, 2009). Many mechanisms have been proposed to trigger the LPE event, including Siberian flood basalt volcanism, sea level change, extraterrestrial impact, ocean deoxygenation, water column stratification and climate change driven by methane hydrate collapse (Campbell et al., 1992; Wignall and Hallam, 1992; Renne et al., 1995; Becker et al., 2001; Benton and Twitchett, 2003; Kamo et al., 2003). Whatever the trigger or combination of triggers, accumulating evidence points to the rapid deterioration of both the marine and terrigenous ecosystems (Retallack, 1995; Looy et al., 2001; Twitchett et al., 2001; Michaelsen, 2002).

Geochemical techniques have helped to elucidate the nature of the events that unfolded during the Late Permian, yet additional questions have arisen as a result. In addition to a distinctive negative stable carbon isotopic excursion and trace metal enrichment at the boundary (Kaiho et al., 2001, 2006; Cao et al., 2002, 2009), anomalous distributions of lipid biomarkers, including isorenieratane and derived aryl isoprenoids, 2-methylhopanes and crocetane, are defining features of the PTB (Grice et al., 2005; Wang et al., 2005; Xie et al., 2005; Wang, 2007; Cao et al., 2009). Additionally, anomalous values of molecular ratios, including  $C_{30}$  17 $\beta$ ,21 $\alpha$ (H)-hopane/ $C_{30}$  17 $\alpha$ ,21 $\beta$ (H)-hopane (referred to as the  $C_{30}$  moretane/hopane ratio),  $C_{27}$  18 $\alpha$ -trisorhopane/ $C_{27}$  17 $\alpha$ -trisorhopane (referred to as Ts/(Ts + Tm)), Tm/ $C_{30}$  hopane,  $C_{31}/C_{32}$  hopane,  $C_{35}$  Homohopane Index ( $C_{35}$  HHI), and hopane/sterane, are recorded in sediments deposited at the PTB (Wang, 2007; Xie et al., 2007; Cao et al., 2009).

Multiple scenarios have been proposed to explain the elevated moretane/hopane ratios at the PTB. Geochemical maturity parameters throughout the Meishan GSSP section in southeastern China are nearly uniform, and thus, thermal maturity variations cannot adequately explain the moretane/hopane and Ts/(Ts + Tm) variability observed through the section (Cao et al., 2009). Accordingly, additional mechanisms have been proposed to account for the moretane variability, including increased input of higher plant organic matter to the marine system, increased acidification, freshening of the upper water column, or lithological effects (Wang, 2007; Xie et al., 2007; Cao et al., 2009).

In order to further assess and correctly interpret the moretane anomalies at the PTB, homohopane, 2 $\alpha$ - and 3 $\beta$ -methylhomohopane and lithological data for a drill core taken from the Meishan section in China were critically examined. The possible mechanisms for generating the observed moretane record, including thermal maturity, source input, redox conditions, and lithology, were examined in light of the new hopane and lithological data.

### 1.1. Moretane background

Hopanes are pentacyclic triterpanes and are arguably the most ubiquitous natural product found on Earth (Ourisson and Albrecht, 1992). Bacteria are the dominant source of hopanes in marine sediments, and bacteriohopanepolyols (BHP) are the primary precursor of  $C_{30}$  and higher hopane homologues. Hopanes have readily isomerized asymmetric carbon atoms at C-17 and C-21, where  $\alpha$  and  $\beta$  denote whether the hydrogen is below or above the plane of the ring system, respectively. Consequently, when considering C-17 and C-21, there are four possible stereoisomers (Fig. 1): 17 $\beta$ ,21 $\beta$ (H)-hopane ( $\beta\beta$ -hopane), 17 $\beta$ ,21 $\alpha$ (H)-hopane ( $\beta\alpha$ -moretane), 17 $\alpha$ ,21 $\beta$ (H)-hopane ( $\alpha\beta$ -hopane), and 17 $\alpha$ ,21 $\alpha$ (H)-hopane ( $\alpha\alpha$ -hopane; this isomer is not generally encountered in sediments). The term "moretane" distinguishes the 17 $\beta$ ,21 $\alpha$ (H)-hopane stereoisomers from the other hopane stereoisomers, while the others are simply referred to as 'hopanes'. The  $\beta\beta$ -hopanoids are the commonly observed biological configuration and are found in bacterial cultures and immature organic material. The  $\beta\beta$  configuration is nearly planar, which enables the molecule to fit into the membrane lipid bilayer (Peters et al., 2005), but the  $\beta\beta$ -hopane is the least thermodynamically stable of the hopane stereoisomeric series (Seifert and Moldowan, 1980; Kolaczowska et al., 1990; Peters et al., 2005). During diagenesis and catagenesis,  $\beta\beta$ -hopane is removed by thermal degradation or interconversion to the more thermodynamically stable  $\beta\alpha$ -moretane and  $\alpha\beta$ -hopane. According to the scheme illustrated in Seifert and Moldowan (1980),  $\beta\alpha$ -moretane can overcome an energy barrier given sufficient thermal energy to be converted to the thermodynamically preferred  $\alpha\beta$ -hopane via the  $\beta\beta$ -hopane intermediate (Peters et al., 2005). The  $\alpha\alpha$ -hopane is less thermodynamically stable than either 17 $\beta$ ,21 $\alpha$ (H)-moretane or 17 $\alpha$ ,21 $\beta$ (H)-hopane, and it is largely undetected in petroleum and mature petroleum source rocks (Bauer et al., 1983; Kolaczowska et al., 1990).

The distributions of terpane isomers can be used to estimate thermal maturity. Predictions of thermodynamic stability of the different hopane stereoisomeric series and observations of the degree of isomerization of hopanes in immature organic matter and petroleum have led to use of the  $\beta\alpha$ -moretane to  $\alpha\beta$ -hopane ratio as a thermal maturity indicator (Seifert and Moldowan, 1980; Peters et al., 2005). The  $\beta\alpha$ -moretane/ $\alpha\beta$ -hopane ratio is used to characterize immature to mildly mature oils. However, thermal maturity is not the only factor that influences the  $\beta\alpha$ -moretane/ $\alpha\beta$ -hopane ratio. The source of organic matter input and depositional environment influence the terpane fingerprint of petroleum and can significantly affect thermal maturity parameters (Peters et al., 2005). Based on reports

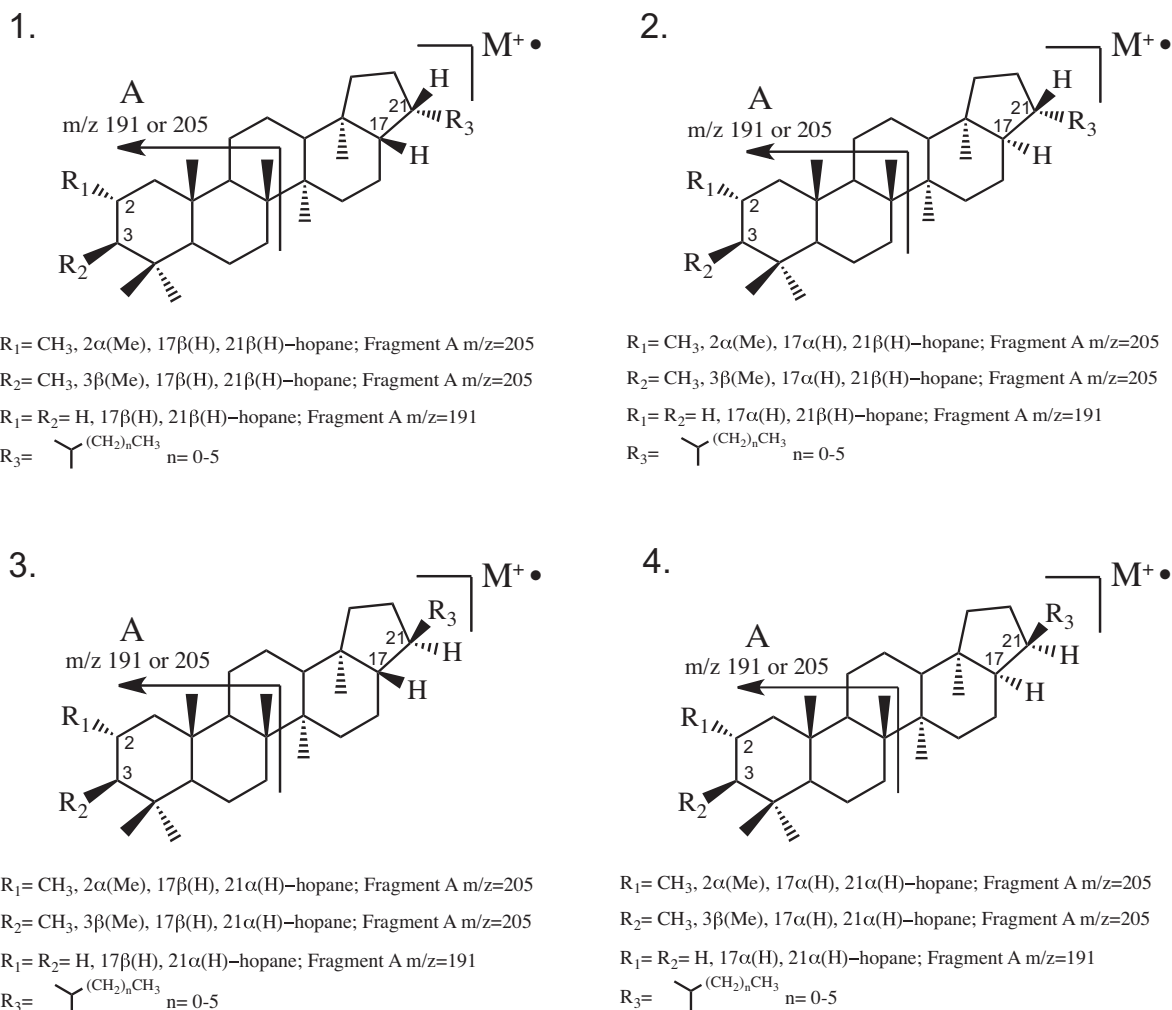


Fig. 1. Structures of the  $\beta\beta$ -hopanoid (1),  $\alpha\beta$ -hopanoid (2),  $\beta\alpha$ -hopanoid (3), and the  $\alpha\alpha$ -hopanoid (4) series are illustrated. Key asymmetric carbon atoms of interest are labeled. The mass spectrometry fragment A is marked with the expected mass units depending on methylation. The molecular ion is indicated and has an expected mass of 412 for  $\text{C}_{30}$  hopane up to 482 for  $\text{C}_{35}$  hopanes.

of  $17\beta, 21\alpha(\text{H})$  hopanoids in hypersaline environments, peat, coal, lacustrine environments, and in living systems (Quirk et al., 1984; Rullkötter and Marzi, 1988; Uemura and Ishiwatari, 1995; Rosa-Putra et al., 2001), some authors have invoked increased input of higher plant organic matter to explain anomalous moretane abundance in marine sediments where thermal maturity is not the cause of variability (Grantham, 1986; Isaksen and Bohacs, 1995; Wang, 2007; Xie et al., 2007). However, in a number of instances, depositional environment has been shown to strongly modulate terpane distributions, including the abundance of moretane relative to  $\alpha\beta$ -hopane (Peters et al., 2005).

## 2. SAMPLES AND EXPERIMENTAL METHODS

### 2.1. Geographic setting

The Meishan quarries in South China have produced detailed information about the Permian–Triassic mass extinction. The Meishan section is the Global Stratotype

Section and Point (GSSP) for the PTB, as well as for the base of Changhsingian Stage. In order to avoid sampling material that was altered and contaminated during surficial weathering, a drilling project was undertaken by the Nanjing Institute of Geology and Paleontology in 2004. A detailed description of the Meishan section and the drilling project are provided in the supplementary online material of Cao et al. (2009).

### 2.2. Biomarker analyses

As described by Cao et al. (2009), the exterior of the samples were brushed clean and rinsed with methanol (MeOH) and dichloromethane (DCM) prior to being powdered using a solvent-cleaned ceramic puck mill. Procedural blanks were prepared along with the samples and showed no evidence of laboratory contamination. Samples were solvent extracted using a Dionex ASE-200 extractor and a solvent mixture of DCM and MeOH (9:1). Elemental sulfur was removed from the total lipid extracts using acid-washed copper granules. Aliphatic, aromatic, and polar fractions

were collected by silica column chromatography using hexane, hexane/DCM (4:1), and DCM/MeOH (4:1) solvents, respectively.

Each fraction was dried and weighed before adding analytical standards to 1 mg of the saturated fraction. The saturated hydrocarbon biomarkers were analyzed by gas chromatography–mass spectrometry (GC–MS) in full scan and metastable reaction monitoring (MRM) modes. The characteristic  $m/z$  191 and 205 mass fragments were used to identify the  $C_{30}$ – $C_{34}$  homohopanes and  $2\alpha$ - and

$3\beta$ -methylhopanes in MRM mode, respectively (see Fig. 2). The 22S and 22R isomers of  $C_{31}$ – $C_{34}$  homohopanes and  $C_{32}$ – $C_{33}$  methylhomohopanes were identified, and both isomers were used in the calculation of the  $\beta\alpha/(\beta\alpha + \alpha\beta)$  ratios. The 22S and 22R isomers of  $\beta\alpha$ - $C_{31}$  homohopane and  $\beta\alpha$ - $C_{32}$  methylhomohopane coelute, so these compounds were integrated as a single peak as illustrated in Fig. 2. The supplementary online material of Cao et al. (2009) describes the biomarker analytical methods in greater detail.

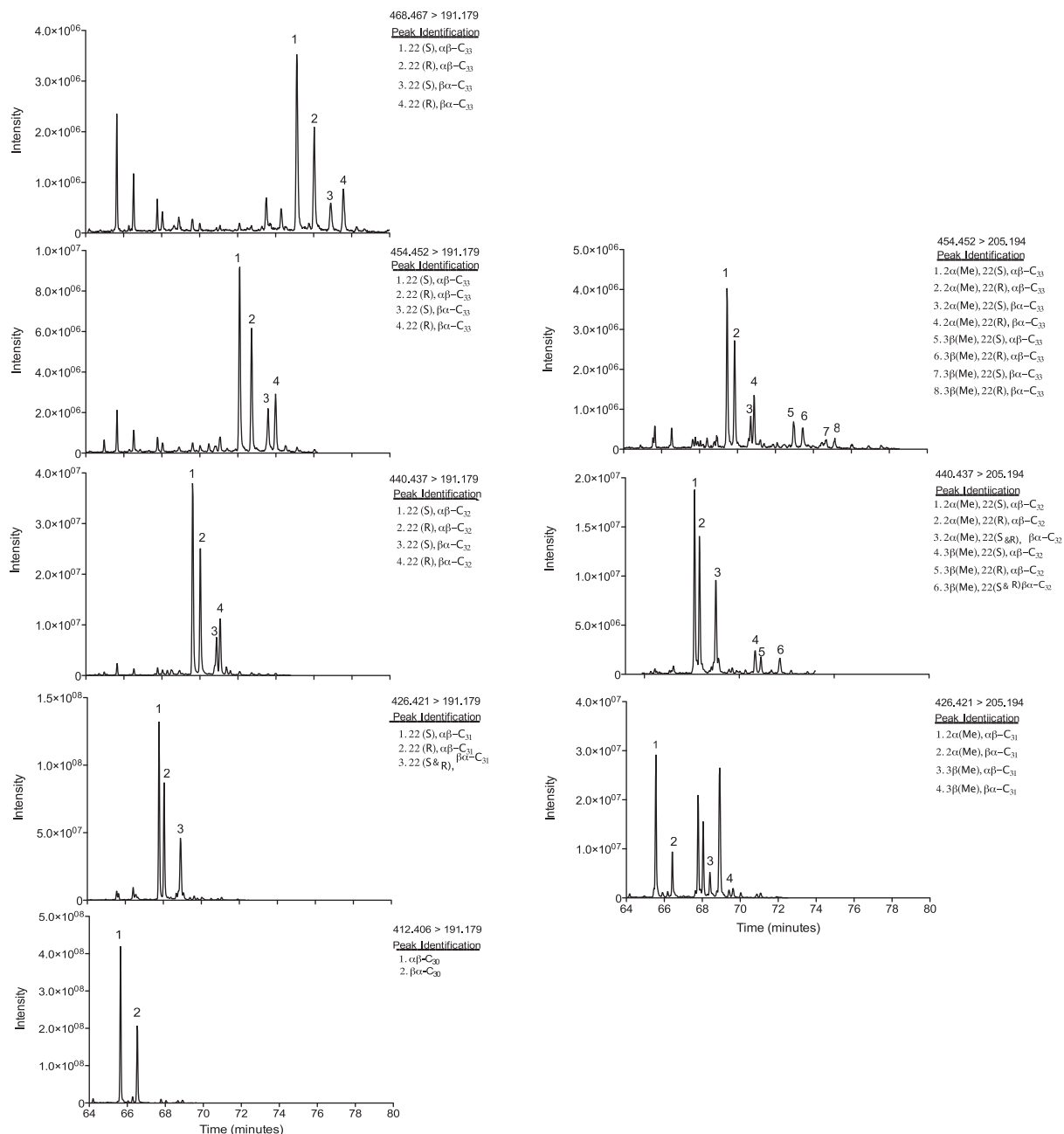


Fig. 2. Multiple reaction monitoring (MRM) chromatograms from sample MS-core1-35-1 at 94.53 m depth are shown. The MRM transitions are written to the right of the chromatogram. In the left column, the 191.179 fragment corresponds to the A/B rings for homohopanes (see Fig. 1). In the right column, the 205 mass fragment corresponds to the A/B ring fragment for  $2\alpha$ - and  $3\beta$ -methylhomohopanes. All peaks are marked numerically with the corresponding identification to the right.

### 2.3. Mineralogical analyses

#### 2.3.1. Carbonate contents

Approximately 0.5 g of each powdered sample was accurately weighed into a clean Teflon tube. Methanol was added to wet the sample prior to acidification. Each sample was acidified with a 10% aqueous hydrochloric acid (HCl) solution. The samples were treated again with a 15% HCl solution and left for 24 h to allow the reaction to reach completion. The samples were rinsed with water five times to remove any remaining acid before being dried in a 60 °C oven for 48 h. The samples were reweighed, and the percentage carbonate was calculated based on the difference between the initial and final weights.

#### 2.3.2. Clay analyses

Preparation for bulk mineralogical analysis of all samples involved crushing rock samples in an agate swing mill, addition of 10 wt.% ZnO and further milling to ensure mixing and homogeneous distribution. Bulk mineralogical analysis was performed on randomly oriented samples using a Bruker D8 X-ray diffractometer at 40 kV and 30 mA with CuK $\alpha$  radiation. Analyses were performed from 2–65° 2 $\theta$  (for any diffracted X-ray obeying Bragg's Law, 2 $\theta$  as referred to herein is equal to two times the angle between the sample plane and the incident X-ray beam) at a step size of 0.02° and counting times of 4 s per step. Quantitative analysis was performed with single line and full profile fitting using pure mineral standards for reference intensity ratios (Srodon et al., 2001).

Determination of clay mineralogy involved light crushing of samples by hand in a steel mortar and pestle and for samples containing appreciable carbonate content, decarbonation with 1 M acetic acid while monitoring pH. Decarbonated samples were rinsed three times with deionised water and all samples were resuspended with sodium phosphate, sonicated and the <2 and <0.2  $\mu$ m size fractions were obtained by timed centrifugation. Centrifuged samples were decanted and oriented Ca-saturated aggregates were prepared by using a filter membrane technique and transfer of clay films for glass substrates. X-ray diffraction was performed using a Siemens D5000 diffractometer at 30 kV and 20 mA, with CuK $\alpha$  radiation from 2–35° 2 $\theta$  a step size of 0.03° and counting times of 8–10 s. Divergence, receiving and anti-scatter slits were 0.2 and 1 mm in size, respectively, and a Ni filter was used. Clay samples were analysed in the air-dried Ca-saturated state, after ethylene glycol solvation overnight at 60 °C (to identify expandable minerals), heating at 400 °C for 2 h (to quantify collapsible/expanding mineral proportions), and heating to 550 °C for 2 h (to aid in quantifying kaolinite and chlorite proportions). Relative clay abundances were determined by peak area measurement, expressed in relative percent and normalized to total clay content by total clay mineral abundance determined by bulk mineralogical analyses. The composition of mixed-layered species was determined using one dimensional X-ray diffraction pattern modeling with the software package NEWMOD (Reynolds and Reynolds, 1996).

### 3. RESULTS

#### 3.1. Stratigraphic variation of lithology and hopane distributions

The  $\beta\alpha/(\beta\alpha + \alpha\beta)$  ratios for C<sub>30</sub> hopane, C<sub>31–34</sub> homohopanes, C<sub>31–33</sub> 2 $\alpha$ -methylhopanes, and C<sub>31–33</sub> 3 $\beta$ -methylhopanes were calculated for each sample (Table 1). The precise determination of  $\beta\alpha/(\beta\alpha + \alpha\beta)$  for the C<sub>31</sub> and C<sub>32</sub> 3 $\beta$ -methylhopanes was precluded by interfering peaks and will not be further discussed. The  $\beta\alpha/(\alpha\beta + \beta\alpha)$  values vary from 0.04 to 0.34 for all of the other hopane series measured. The profiles of C<sub>30</sub> hopane, the homohopanes, and the 2 $\alpha$ - and 3 $\beta$ -methylhomohopanes show parallel down-core trends and similar values (Fig. 3). Ts/(Ts + Tm) and C<sub>35</sub> Homohopane Index (HHI) data from Cao et al. (2009) were plotted in Fig. 3 for comparison. Notably, the rocks record three positive moretane enrichments. The first interval of enhanced moretane/hopane ratios occurs in the Lungtan Formation, followed by the second interval at the PTB in the Yinkeng Formation, and the last interval of moretane enrichment at the end of the Griesbachian in the Helongshan Formation.

The bulk lithology, including percent carbonate, total clay, and quartz was determined (Table 2). The lithology was highly variable through the drill core section (Fig. 4). The percent carbonate fluctuates from 8.5% to 99%. The percent total clay and the percent quartz both vary from close to 0% to nearly 50%. The Lungtan Formation is a clay-rich unit that is enriched in quartz and is characterized by low carbonate (8.5–14%). The percent carbonate increases significantly in the overlying Changxing unit, although the carbonate and quartz percentages are more variable through this interval. Unlike the Lungtan Formation, clay is a minor component through the Changxing Formation. The percent total clay returns to elevated values in the Yinkeng Formation, while the percent carbonate is significantly lower than the Changxing or Helongshan formations. Through the Helongshan Formation, the samples are all over 95% carbonate with very little clay or quartz. Similar to the observations of Rullkötter and Marzi (1988), elevated abundances of moretanes relative to  $\alpha\beta$ -hopane are associated with carbonate-poor facies.

Further clay mineralogical analyses provided the absolute and relative percentages of specific clay types, including illite, chlorite, smectite, kaolinite, berthierine, and mixed layer illite/smectite (Table 3). The total percent clay and the absolute and relative percentages of the clay type varied through the section (see Fig. 5). Illite and mixed layer illite/smectite represent the dominant clay types, where the sum of percent illite and mixed layer illite/smectite represents over 50% through the entire section. The relative percentage of illite/smectite mixed layer clay is largely constant throughout the clay mineral assemblage. Although more variable, kaolinite, chlorite, and smectite clays become a significant fraction of the total clay through some intervals of the assemblage. Notably, berthierine, which is usually formed under reducing conditions (Taylor and Curtis, 1995; Fritz and Toth, 1997), is present in the Lungtan Formation at the base of the section. Measurable differ-

Table 1  
Summary of geochemical data.

Sample ID	Drilling depth (m)	C <sub>30</sub> βα/ (βα + αβ)	C <sub>31</sub> βα/ (βα + αβ)	C <sub>32</sub> βα/ (βα + αβ)	C <sub>33</sub> βα/ (βα + αβ)	C <sub>34</sub> βα/ (βα + αβ)	2α Me C <sub>31</sub> βα/ (βα + αβ)	2α Me C <sub>32</sub> βα/ (βα + αβ)	2α Me C <sub>33</sub> βα/ (βα + αβ)	3β Me C <sub>33</sub> βα/ (βα + αβ)
MS05-140	7.05	0.069	0.101	0.067	0.075	0.080	0.070	0.104	0.037	0.103
MS05-165	31.05	0.059	0.092	0.060	0.074	0.043	0.045	0.111	–	–
MS05-170	39.56	0.138	0.151	0.122	0.129	0.133	0.135	0.142	0.112	0.140
MS05-175	46.79	0.060	0.098	0.041	0.054	0.063	0.047	0.092	–	–
MS05-180	61.77	0.118	0.135	0.103	0.098	0.088	0.091	0.151	0.098	0.113
MS05-200	89.71	0.152	0.140	0.140	0.145	0.134	0.154	0.209	0.132	0.189
MS-1-core 36-3	92.61	0.335	0.223	0.227	0.267	0.246	0.302	0.304	0.244	0.260
MS-1-core 35-1	94.53	0.343	0.228	0.233	0.267	0.221	0.329	0.290	0.238	0.234
MS-1-core 34-3	102.59	0.300	0.197	0.210	0.222	0.226	0.298	0.263	–	0.205
MS05-2b	111.44	0.053	0.043	0.036	0.075	0.070	0.064	0.078	–	–
MS05-10	116.51	0.048	0.088	0.041	0.050	0.090	0.075	0.087	0.052	0.068
MS05-30	127.82	0.048	0.103	0.057	0.055	0.048	0.084	0.102	0.056	0.062
MS05-60	147.08	0.045	0.092	0.035	0.043	0.041	0.055	0.088	0.030	0.121
MS05-76	157.48	0.052	0.085	0.039	0.053	0.044	0.063	0.083	0.045	0.045
MS05-92b	169.24	0.045	0.084	0.044	0.052	0.046	0.046	0.079	0.056	0.067
MS05-117	186.91	0.211	0.172	0.168	0.176	0.168	0.208	0.227	0.193	0.177
MS05-134	208.22	0.222	0.170	0.175	0.180	0.163	0.271	0.251	0.200	0.165
MS05-136c	211.3	0.188	0.161	0.146	0.165	0.155	0.190	0.226	0.220	0.157
MS05-138	213.52	0.073	0.090	0.057	0.066	0.051	0.080	0.088	0.054	0.093

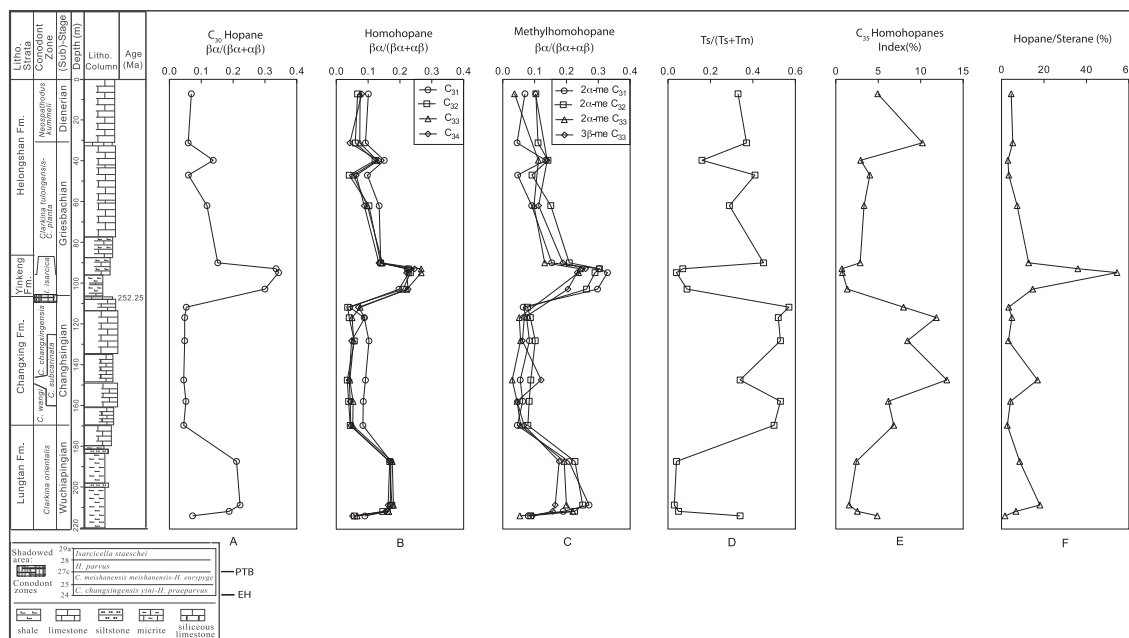


Fig. 3. Vertical profiles of molecular parameters, including the moretane/hopane ratio ( $\beta\alpha/(\beta\alpha + \alpha\beta)$ ) of  $C_{30}$  (A), the homohopane series (B), the  $2\alpha$ - and  $3\beta$ -methylhomohopanes (C),  $Ts/(Ts + Tm)$  (D), the  $C_{35}$  homohopane index (%) (E), and hopane/sterane (%) (F), are plotted versus the stratigraphic column (modified from Cao et al. (2009)). The  $Ts/(Ts + Tm)$ ,  $C_{35}$  HHI, and hopane/sterane data are from Cao et al. (2009). The three moretane/hopane excursions occur at 39.56, 92.61–102.59, and 186.91–213.52 m. The legend for the stratigraphic column is at bottom right. In the expanded view of the conodont zones in the legend, the PTB is marked according to the first appearance of the conodont *Hindeodus parvus*, and the extinction horizon (EH) is marked at the top of bed 24.

Table 2  
Bulk lithology.

Sample ID	Percent clay	Percent carbonate	Percent quartz	Percent other
MS05-140	0.12	99.03	0.85	0.00
MS05-165	0.16	99.02	0.82	0.00
MS05-170	2.74	96.19	1.07	0.00
MS05-175	2.52	96.61	0.74	0.13
MS05-180	1.37	98.48	0.11	0.04
MS05-200	41.55	14.59	42.76	1.11
MS-1-core 36-3	45.03	20.44	28.13	6.41
MS-1-core 35-1	47.86	16.49	29.28	6.38
MS-1-core 34-3	49.75	14.42	31.43	4.41
MS05-2b	2.01	82.21	15.79	0.00
MS05-10	0.49	90.67	8.84	0.00
MS05-30	6.90	44.46	48.52	0.12
MS05-60	1.83	62.04	36.08	0.05
MS05-76	0.00	77.66	22.35	0.00
MS05-92b	0.27	91.70	8.03	0.00
MS05-117	43.64	8.54	42.81	5.00
MS05-134	26.33	10.32	58.64	4.71
MS05-136c	38.83	11.40	42.84	6.93
MS05-138	2.64	13.76	78.86	4.74

Note: See Table 1 for sample depths.

ences between the glycolated and heated (400 °C) samples in the 7 Å peak suggest that trace abundances of berthierine may be present in the samples between 92 and 103 m. It is not possible to determine from our results whether the berthierine is detrital or authigenic.

### 3.2. Crossplots of molecular indices and lithological data

Cross-correlation diagrams were generated to evaluate the relationships between the geochemical and lithological data. The  $\beta\alpha/(\alpha\beta + \beta\alpha)$  ratios of  $C_{30}$  hopane were plotted

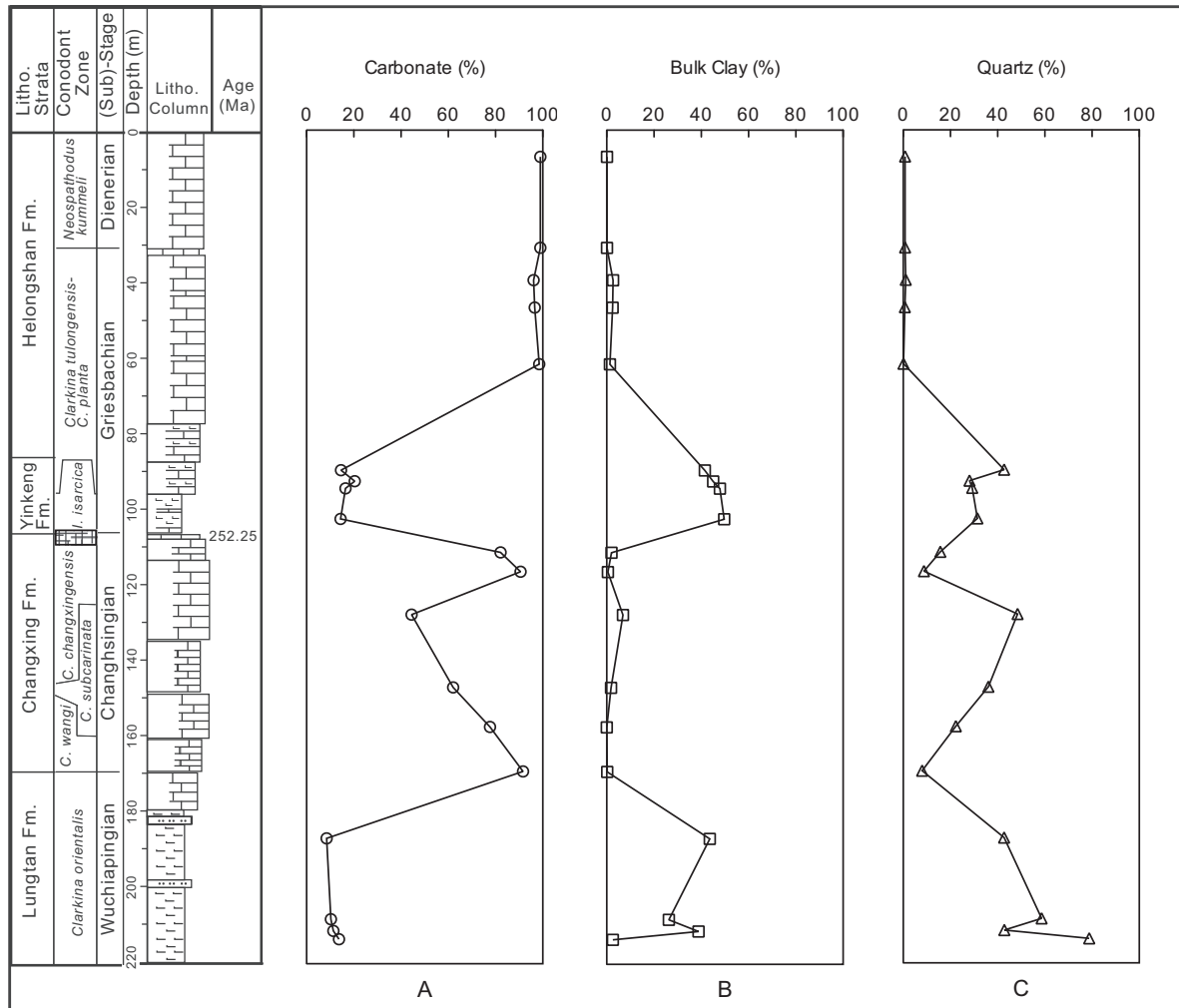


Fig. 4. Vertical profiles of the bulk lithological components by percentage versus the stratigraphic column (modified from Cao et al., 2009). (A) percentage carbonate; (B) percentage total clay; (C) percentage quartz. See Fig. 3 for the stratigraphic column legend.

against the  $\beta\alpha/(\alpha\beta + \beta\alpha)$  ratios of  $C_{31}$ – $C_{34}$  homohopanes and the  $2\alpha$  and  $3\beta$ -methylhomohopanes (Fig. 6A and B). In both cases, an excellent positive correlation is observed with  $R^2$  values ranging from 0.88 to 0.99. Cao et al. (2009) found that  $Ts/(Ts + Tm)$  varied inversely with the  $C_{30}$  hopane  $\beta\alpha/(\alpha\beta + \beta\alpha)$  ratio. Likewise, the  $Ts/(Ts + Tm)$  data reported by Cao et al. (2009) also correlate inversely with the homohopane and  $2\alpha$ - and  $3\beta$ -methylhomohopane  $\beta\alpha/(\alpha\beta + \beta\alpha)$  ratios with  $R^2$  values ranging from 0.64 to 0.77 (Fig. 6C and D).

The carbonate percentage and total clay percentage were plotted against the moretane/hopane ratios for all of the hopane series and  $Ts/(Ts + Tm)$  (Fig. 7). The percent carbonate and percent clay have opposite relationships with the  $\beta\alpha/(\alpha\beta + \beta\alpha)$  ratios. Carbonate percentage and the  $\beta\alpha/(\alpha\beta + \beta\alpha)$  ratios of all of the hopane series are inversely related, having  $R^2$  values ranging from 0.42 to 0.57. The correlation is significantly improved with  $R^2$  values from 0.74 to 0.87 when the  $\beta\alpha/(\alpha\beta + \beta\alpha)$  ratios are plotted against total clay percentage. Similarly, the correlation of  $Ts/(Ts + Tm)$  with the total clay percentage ( $R^2 = 0.52$ ) is stronger than with the percent carbonate ( $R^2 = 0.36$ ). However, the  $R^2$  val-

ues for  $Ts/(Ts + Tm)$  versus carbonate and total clay percentages are less than for the  $\beta\alpha/(\alpha\beta + \beta\alpha)$  ratios in both cases.

The  $\beta\alpha/(\alpha\beta + \beta\alpha)$  ratios for all of the hopane series were plotted together with the percentages of the different clay types in Fig. 8. Like the total clay percentage, all of the clay types were directly related to  $\beta\alpha/(\alpha\beta + \beta\alpha)$ , yet some clay types were more strongly correlated to  $\beta\alpha/(\alpha\beta + \beta\alpha)$  than others. Kaolinite had the weakest correlation with  $\beta\alpha/(\alpha\beta + \beta\alpha)$ , having  $R^2$  values from 0.024 to 0.222. Likewise, smectite was weakly correlated to  $\beta\alpha/(\alpha\beta + \beta\alpha)$ , having  $R^2$  values spanning 0.215–0.485. On the other hand, the percent chlorite was strongly correlated with  $\beta\alpha/(\alpha\beta + \beta\alpha)$ , where  $R^2$  values ranged from 0.773 to 0.901. Percent illite and percent mixed layer illite/smectite also yielded strong correlations with  $\beta\alpha/(\alpha\beta + \beta\alpha)$ .

The  $Ts/(Ts + Tm)$  values from Cao et al. (2009) were plotted versus the different types of clays. Low values of  $Ts/(Ts + Tm)$  occur during intervals of high clay accumulation, in particular, intervals where chlorite, illite, and illite/smectite mixed layer clays comprise a higher proportion of rock lithology. The  $R^2$  values for  $Ts/(Ts + Tm)$  were less

Table 3  
Absolute and relative clay type percentages.

Sample ID	Absolute percent illite	Absolute percent berthierine	Absolute percent kaolinite	Absolute percent chlorite	Absolute percent illite/smectite mixed layer	Absolute percent smectite
MS05-140	0.068	0.000	0.013	0.006	0.038	0.000
MS05-165	0.058	0.000	0.061	0.000	0.044	0.000
MS05-170	1.448	0.000	0.000	0.476	0.807	0.004
MS05-175	1.301	0.000	0.008	0.423	0.786	0.000
MS05-180	0.634	0.000	0.000	0.204	0.530	0.001
ms05-200	14.703	0.000	0.272	3.384	13.233	9.958
ms-1-core 36-3	14.522	0.000	0.000	6.874	18.355	5.274
ms-1-core 35-1	17.344	0.000	0.000	9.380	13.921	7.212
ms-1-core 34-3	16.424	0.000	0.005	8.311	15.274	9.731
ms05-2b	0.261	0.000	0.252	0.000	1.494	0.000
MS05-10	0.248	0.000	0.065	0.000	0.173	0.000
MS05-30	0.758	0.000	2.142	0.000	3.999	0.000
MS05-60	0.281	0.000	0.905	0.000	0.646	0.000
MS05-76	0.000	0.000	0.000	0.000	0.000	0.000
MS05-92b	0.105	0.000	0.055	0.000	0.112	0.000
MS05-117	7.395	2.427	7.534	6.213	20.053	0.023
MS05-134	6.338	2.666	4.748	3.564	9.004	0.013
MS05-136c	11.535	3.831	5.408	5.835	12.201	0.021
MS05-138	0.681	0.301	0.009	0.963	0.690	0.000
	Relative percent illite	Relative percent berthierine	Relative percent kaolinite	Relative percent chlorite	Relative percent illite/smectite mixed layer	Relative percent smectite
MS05-140	54.38	0.00	10.70	4.43	30.46	0.03
MS05-165	35.84	0.00	37.17	0.00	26.99	0.00
MS05-170	52.95	0.00	0.00	17.42	29.49	0.14
MS05-175	51.67	0.00	0.32	16.81	31.20	0.00
MS05-180	46.33	0.00	0.00	14.90	38.69	0.08
ms05-200	35.39	0.00	0.65	8.14	31.85	23.97
ms-1-core 36-3	32.25	0.00	0.00	15.27	40.77	11.71
ms-1-core 35-1	36.24	0.00	0.00	19.60	29.09	15.07
ms-1-core 34-3	33.02	0.00	0.01	16.71	30.71	19.56
ms05-2b	13.03	0.00	12.54	0.00	74.43	0.00
MS05-10	51.00	0.00	13.29	0.00	35.70	0.00
MS05-30	10.99	0.00	31.04	0.00	57.97	0.00
MS05-60	15.33	0.00	49.43	0.00	35.25	0.00
MS05-76	48.34	0.00	17.55	0.00	34.11	0.00
MS05-92b	38.61	0.00	20.06	0.00	41.18	0.15
MS05-117	16.94	5.56	17.26	14.23	45.95	0.05
MS05-134	24.07	10.12	18.03	13.54	34.19	0.05
MS05-136c	29.71	9.87	13.93	15.03	31.42	0.05
MS05-138	25.75	11.37	0.36	36.41	26.11	0.00

Note: See Table 1 for sample depths.

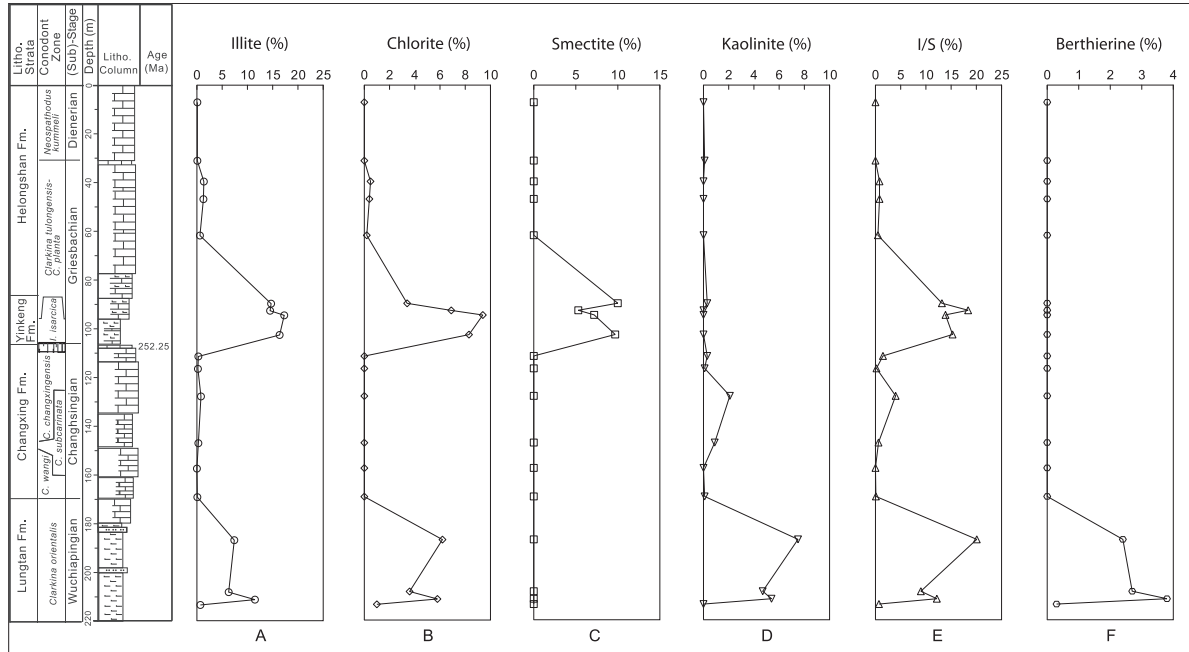


Fig. 5. Vertical profiles of clay types plotted against the stratigraphic column (modified from Cao et al. (2009)). (A) Absolute percent illite; (B) absolute percent chlorite; (C) absolute percent smectite; (D) absolute percent kaolinite; (E) absolute percent mixed layer illite/smectite (I/S); (F) absolute percent berthierine. Note the difference in the x axis scale for clay types. See Fig. 3 for the stratigraphic column legend.

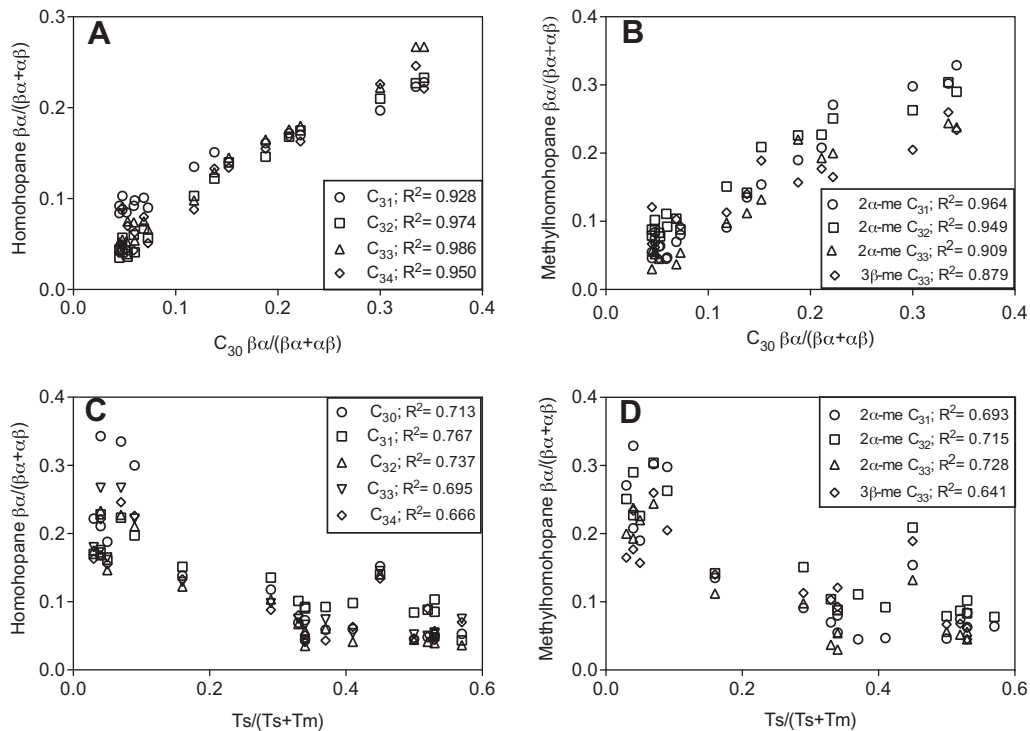


Fig. 6. Cross-correlations of molecular indices. Plots A and B relate moretane/hopane of the  $C_{30}$  hopane to the higher homologues of the homohopane series and  $2\alpha$ - &  $3\beta$ -methylhomohopane series, respectively. Plots C and D relate  $Ts/(Ts + Tm)$  to the higher homologues of the homohopane series and  $2\alpha$ - and  $3\beta$ -methylhomohopane series, respectively. The  $R^2$  value associated with the linear regression for each series relationship is given in the legend.

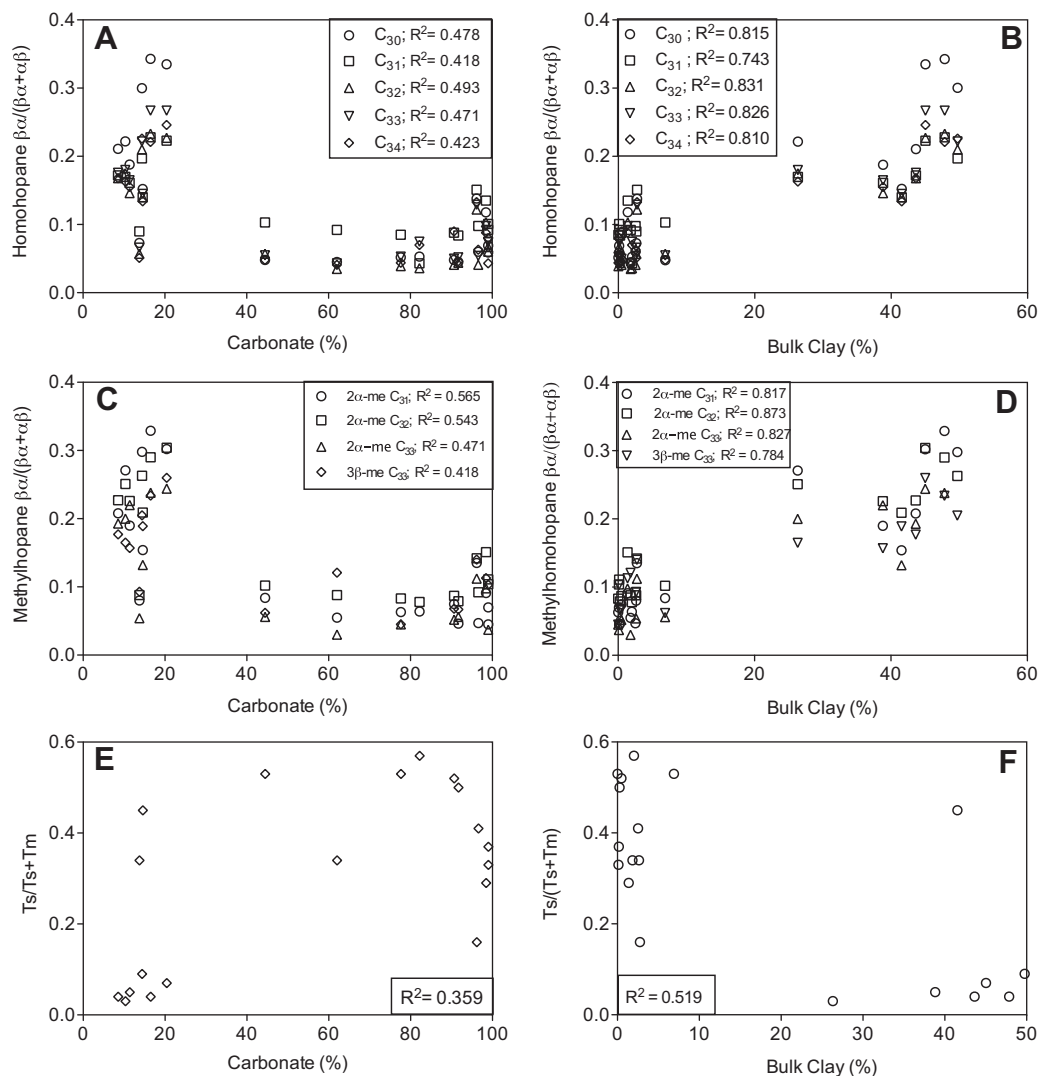


Fig. 7. Cross-correlations of molecular and bulk lithological data. Plots A and B relate carbonate weight percentage and total bulk clay to the homohopane series, respectively. Plots C and D relate carbonate weight percentage and total bulk clay to the  $2\alpha$ - and  $3\beta$ -methylhomohopane series. Plots E and F relate carbonate weight percentage and total bulk clay to  $Ts/(Ts + Tm)$ .

than the  $R^2$  values for the analogous  $\beta\alpha/(\alpha\beta + \beta\alpha)$  plots. Like  $\beta\alpha/(\alpha\beta + \beta\alpha)$ , kaolinite and smectite produced the weakest correlation coefficients, while illite, chlorite, and mixed layer illite/chlorite had higher correlation coefficients with  $Ts/(Ts + Tm)$ .

### 3.3. Crossplots of $C_{35}$ homohopane index and hopane/sterane ratios with moretane/hopane, $Ts/(Ts+Tm)$ and lithological data

The  $C_{35}$  HHI is a redox indicator, and redox conditions are known to affect the distribution of terpanes (Peters et al., 2005). Cross-correlation diagrams were generated to evaluate the relationships between  $C_{35}$  HHI data reported in Cao et al. (2009) and moretane/hopane ratios and  $Ts/(Ts + Tm)$  (Fig. 9). High moretane/hopane ratios for  $C_{30-34}$  homohopanes and  $C_{31-33}$  methylhomohopanes correspond to low values of  $C_{35}$  HHI, which are indicative of oxic conditions. On the other hand, low values of  $Ts/$

$(Ts + Tm)$  correspond with low values of  $C_{35}$  HHI. These results are consistent with previous results relating redox indicators to moretane/hopane ratios and  $Ts/(Ts + Tm)$  (Moldowan et al., 1986; Rullkötter and Marzi, 1988; Wang, 2007). Interestingly, high values of hopane/sterane percentages reported in Cao et al., 2009 correspond with high values of moretane/hopane ratios for  $C_{30-34}$  homohopanes and  $C_{31-33}$  methylhomohopane and low values of  $Ts/(Ts + Tm)$  (Fig. 9). This relationship is unexpected because if the abundance of  $\alpha\beta$ -hopanes were driving the correlation between hopane/sterane ratios and moretane/hopane ratios, one would expect an inverse pattern between these two parameters, which is the opposite of what is observed.

The  $C_{35}$  HHI and hopane/sterane percentages were plotted against total clay percent and all of the clay types detected in the Meishan section (Figs. 10 and 11). In general, the highest values of percent total clay and individual clay types correspond to  $C_{35}$  HHI values less than 5%, but

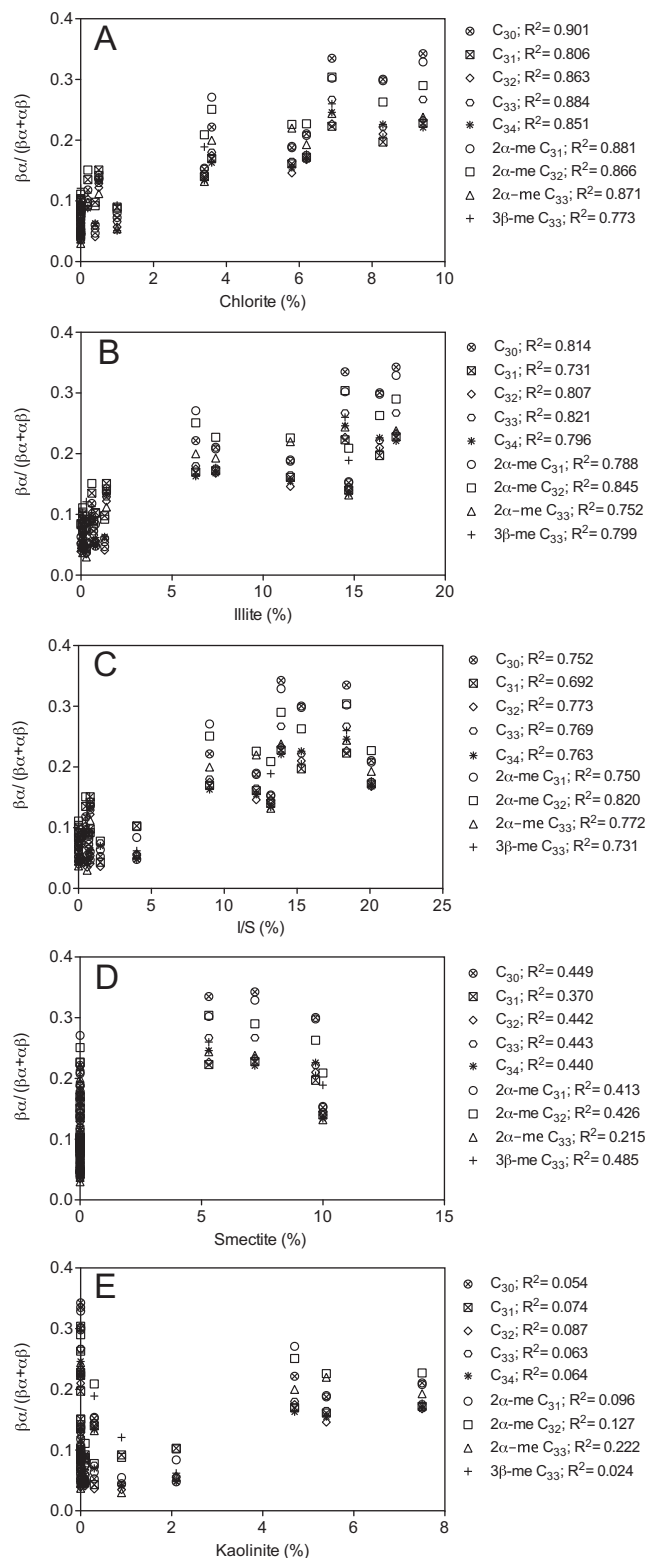


Fig. 8. Correlations between moretane/hopane ratios and the specific clay types are shown for the homohopane and 2 $\alpha$ - and 3 $\beta$ -methylhomohopane series. The  $R^2$  values are listed in the legend next to the corresponding series. (A) Absolute percent chlorite; (B) absolute percent illite; (C) absolute percent mixed layer illite/smectite (I/S); (D) absolute percent smectite; (E) absolute percent kaolinite.

several samples with significant kaolinite abundances have higher C<sub>35</sub> HHI values. High values of hopane/sterane per-

centages are related to high values of total clay, chlorite, illite, mixed layer illite/smectite (I/S), and smectite. Kaolinite

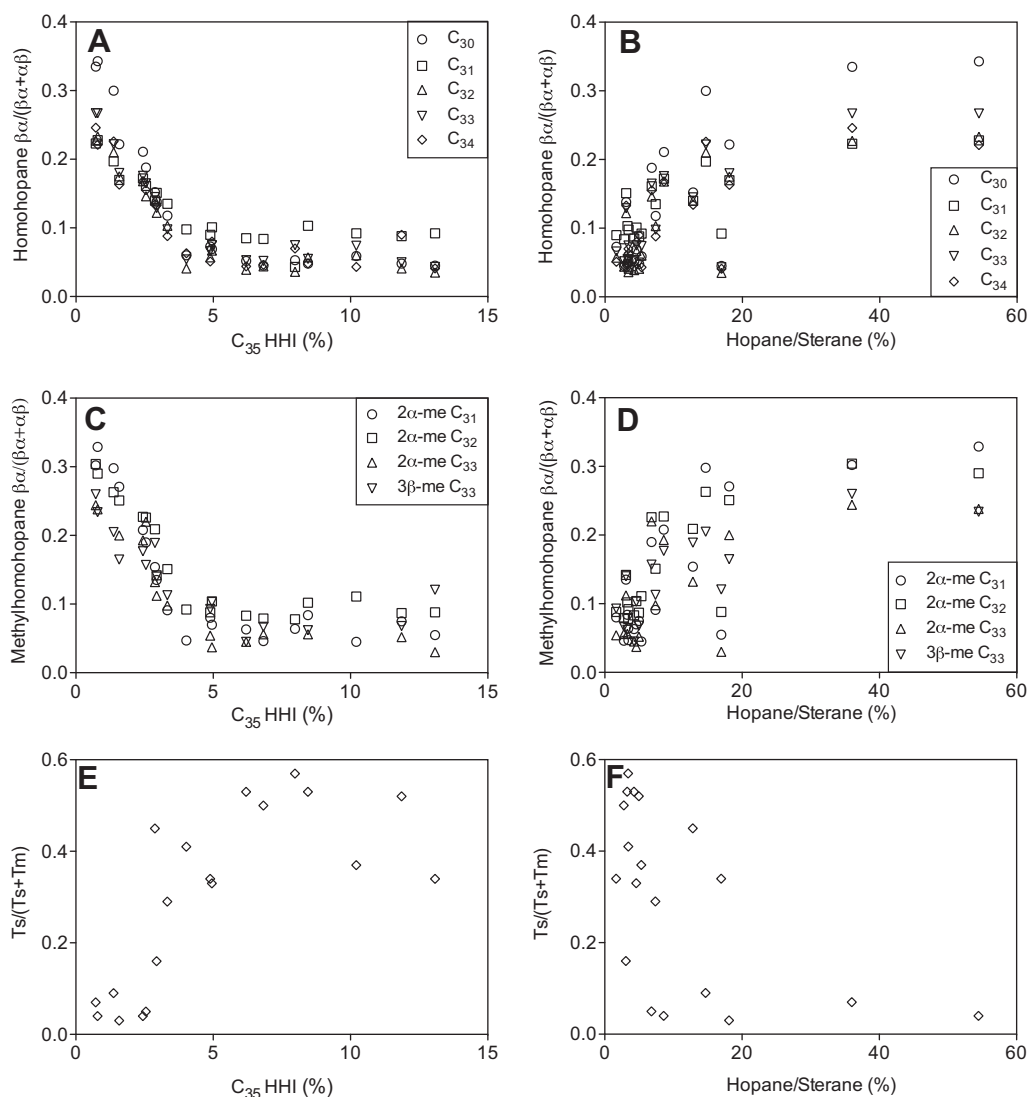


Fig. 9. Correlations of geochemical source and redox indicators against moretane/hopane ratios and  $Ts/(Ts + Tm)$ .  $C_{35}$  HHI (%) vs. homohopanes  $\beta\alpha/(\beta\alpha + \alpha\beta)$  (A), methylhomohopanes  $\beta\alpha/(\beta\alpha + \alpha\beta)$  (C), and  $Ts/(Ts + Tm)$  (E). Hopane/Sterane (%) versus homohopanes  $\beta\alpha/(\beta\alpha + \alpha\beta)$  (B), methylhomohopanes  $\beta\alpha/(\beta\alpha + \alpha\beta)$  (D), and  $Ts/(Ts + Tm)$  (F).

and berthierine do not display this same relationship with the hopane/sterane percentages (see Fig. 11F and G).

#### 4. DISCUSSION

##### 4.1. Possible causes of moretane enrichment

The strong positive correlations between the  $C_{30}$  hopane  $\beta\alpha/(\alpha\beta + \beta\alpha)$  ratios and the homohopane and 2 $\alpha$ - and 3 $\beta$ -methylhomohopane  $\beta\alpha/(\alpha\beta + \beta\alpha)$  ratios imply that the moretane/hopane ratios for all of the hopane series are controlled by the same mechanism, and the mechanism that caused the anomalously high moretane values is not confined or unique to the extinction horizon. Our results show that moretanes are enriched in rocks that are clay-rich and have  $C_{35}$  HHI values indicating oxic conditions, which is consistent with the results of Wang (2007) and Rullkötter and Marzi (1988). Thermal maturity, the source of organic

matter and depositional environment are the three possible factors that can influence the distribution of triterpane isomers (Peters et al., 2005). One or more of these factors is likely responsible for generating the moretane excursions recorded in the Lungtan, Yinkeng and Helongshan formations.

Thermal maturity can be estimated by measuring the degree of isomerization, including the ratio of  $\beta\alpha$ -moretanes to  $\alpha\beta$ -hopanes, the conversion of 22R to 22S for 17 $\alpha$ ,21 $\beta$ (H)-homohopanes and the conversion of 20R to 20S steranes. The moretane to  $\alpha\beta$ -hopane ratio for the  $C_{30}$  compound declines with increasing thermal maturity from  $\sim 0.8$  in immature rocks to  $< 0.15$  for mature rocks (Peters et al., 2005). While the ratio of moretanes to  $\alpha\beta$ -hopanes varies significantly through the drill core, the ratio of 22S/(22S + 22R) for  $C_{31}$  homohopane is between 54% and 59% throughout the entire Meishan drill core (Cao et al., 2009). According to Lacher et al. (1987), these values are

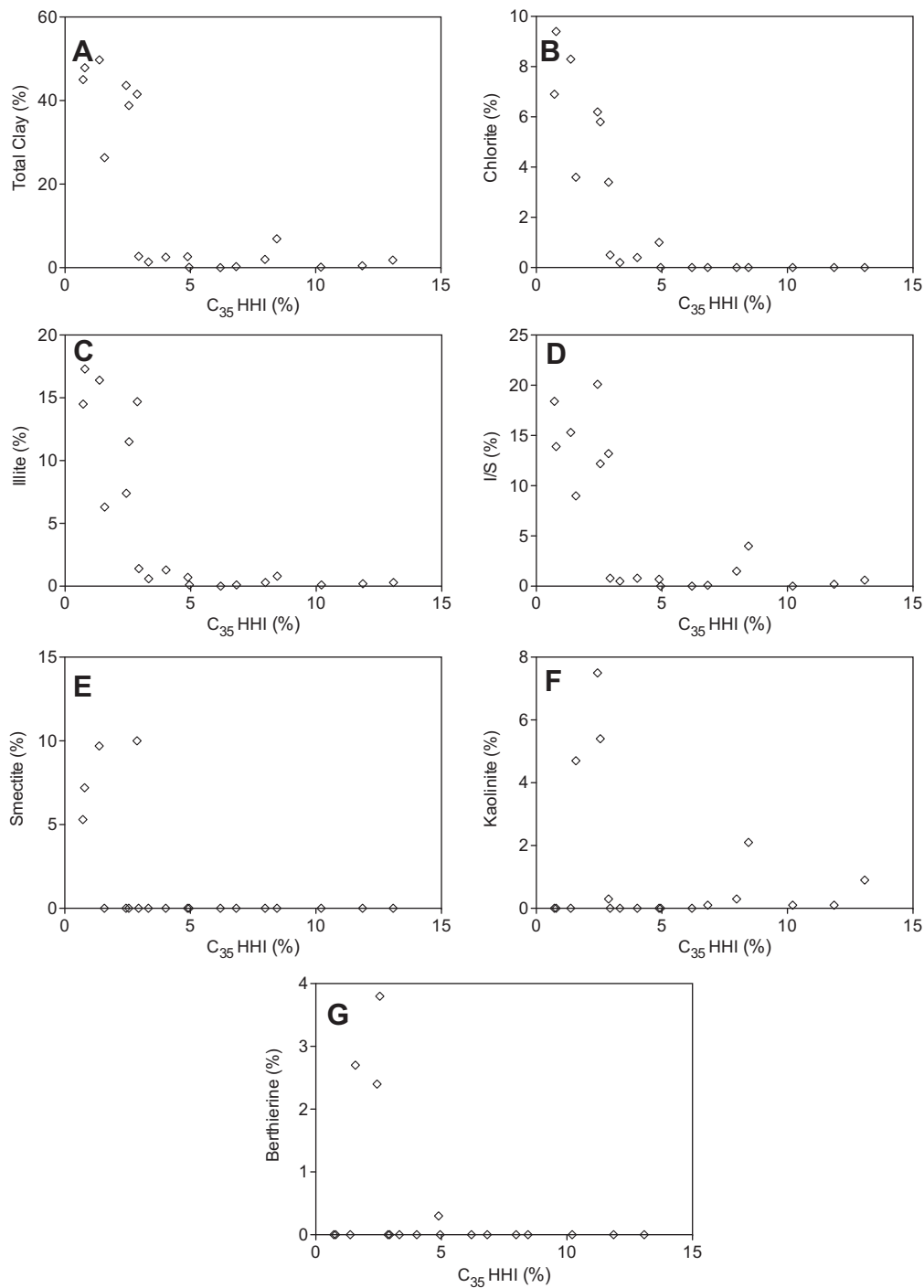


Fig. 10. Correlations of  $C_{35}$  HHI (%), a redox indicator, against percent total clay and clay types.  $C_{35}$  HHI (%) vs. percent total clay (A), absolute percent chlorite (B), absolute percent illite (C), absolute percent illite/smectite mixed layer clay (I/S) (D), absolute percent smectite (E), absolute percent kaolinite (F), absolute percent berthierine (G).

expected for  $\alpha\beta$ -hopanes when the epimerization reaction that converts the biological 22R epimer to 22S has reached the endpoint. The epimerization end point is met before the main phase of oil generation (Peters et al., 2005). The 20S/(20S + 20R) ratios of the  $C_{27}$  steranes varies between 45% and 50%, which further supports the conclusion that the whole cored interval is within the early stages of

petroleum generation and shows little variation throughout (Cao et al., 2009). The largely constant relative percent of illite/smectite mixed layer clay in the section is also consistent with constant thermal maturation throughout the Meishan drill core (Pollastro, 1993). Accordingly, thermal maturity can be ruled out as the factor responsible for moretane variability. Likewise, Wang (2007) and Xie

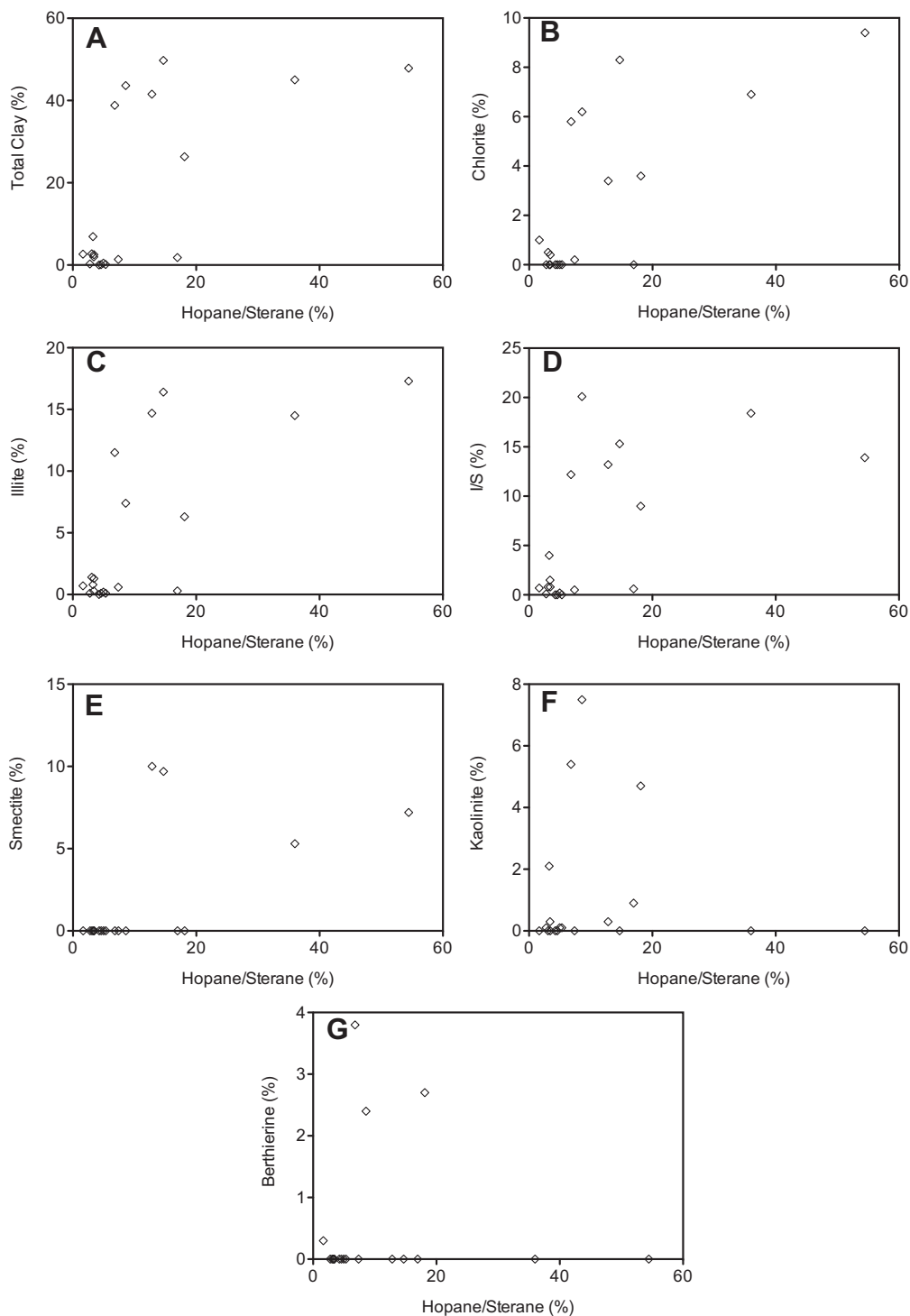


Fig. 11. Correlations of Hopane/Sterane (%), a geochemical source indicator, against percent total clay and clay types. Hopane/Sterane (%) vs. percent total clay (A), absolute percent chlorite (B), absolute percent illite (C), absolute percent illite/smectite mixed layer clay (I/S) (D), absolute percent smectite (E), absolute percent kaolinite (F), absolute percent berthierine (G).

et al. (2007) eliminated thermal maturity as a possible mechanism for generating the moretane anomaly based on additional lines of evidence.

The sources of organic matter profoundly affect biomarker distributions (Peters et al., 2005). Previous studies

have argued that increased terrigenous organic matter input from higher plants, peat, or coal explains elevated moretane/hopane ratios in cases where thermal maturity does not sufficiently explain the pattern of moretane/hopane ratios (Grantham, 1986; Rullkötter and Marzi, 1988; Isaksen

and Bohacs, 1995). The link between moretanes and higher plant organic matter input is based on a series of studies that detected elevated  $\beta\alpha$ -hopanoids in terrigenous influenced sediments and some higher plants. Unusually high abundances of  $17\beta(\text{H})$ ,  $21\alpha$ -moretan-29-ol and  $17\beta(\text{H})$ -moret-22(29)-ene have been reported in acidic and saline lakes (Uemura and Ishiwatari, 1995; Ishiwatari et al., 2005; Aichner et al., 2010; Kristen et al., 2010). Quirk et al. (1984) detected  $\text{C}_{32}$   $\beta\alpha$ -alcohols,  $\text{C}_{31}$  methylmoretan-29-ol, and  $\text{C}_{32}$  and  $\text{C}_{33}$   $\beta\alpha$  hopanoic acids in peat samples, and elevated levels of moretane were reported for coals (e.g., Hughes and Dzou, 1995; Shen and Huang, 2007). Second, although  $\beta\beta$ -hopanes are the presumed biological isomer,  $\beta\alpha$ -hopanoids have been identified in some organisms. The compounds  $21\alpha(\text{H})$ -moret-22(29)-ene ( $\text{C}_{30}\text{H}_{50}$ ) and 30-nor- $21\alpha$ -hopan-22-one (isoadiantone;  $\text{C}_{29}\text{H}_{48}\text{O}$ ) were isolated from ferns and lichens (Hveding-Bergseth et al., 1983; Shiojima and Ageta, 1990; Tsuzuki et al., 2001). Moretenone and moretenol were isolated from a small shrub (Lavie et al., 1968), and Rosa-Putra et al. (2001) discovered that soil bacteria *Frankia* spp. synthesize 22(S)-moretan-29-ol ( $\text{C}_{30}\text{H}_{52}\text{OH}$ ).

Based on the evidence discussed above, some researchers have argued that the PTB moretane anomaly signals increased organic matter input from higher plant material, particularly peat and coal (Wang, 2007; Xie et al., 2007). The data presented in this paper do not support this explanation. None of the previous reports linking higher plant organic matter input to elevated moretane abundances provide a viable explanation for the parallel trends of the extended homohopanes and the  $2\alpha$ - and  $3\beta$ -methylhomohopanes because, with the exception of the peat samples reported by Quirk et al. (1984), the  $\beta\alpha$ -hopanoids detected in organisms, peat, and coal are  $\text{C}_{29}$  or  $\text{C}_{30}$  compounds. Because thermal maturity and a change in input of higher plant organic matter fail to account for the observed moretane anomalies, other source input changes and diagenetic effects must be considered.

Redox potential is known to affect the distribution of terpanes in lipid extracts (Peters et al., 2005). Multiple redox indicators are presented for the Meishan section in Cao et al. (2009). Values of 28,30-dinorhopane (28,30-DNH) between 0.5% and 2% and the detection of isorenieratane and  $\text{C}_{14-27}$  aryl isoprenoids throughout the cored interval indicates that all of the sediments were deposited under reducing conditions. However,  $\text{C}_{35}$  HHI values are highly variable through the drilled interval (0.10–14.47%), which is inconsistent with the multiple redox indicators that suggest reducing conditions throughout the cored interval. Homohopane distribution depends on depositional redox conditions, sulfur incorporation in organic matter, and biodegradation (Peters and Moldowan, 1991). The rocks through the entire cored interval were deposited in a marine setting that likely had the necessary sulfate concentrations required for homohopane distributions to reflect redox conditions. The discrepancy of the  $\text{C}_{35}$  HHI with the other redox indicators and the strong relationship of the  $\text{C}_{35}$  HHI with the moretane/hopane ratios,  $\text{Ts}/(\text{Ts} + \text{Tm})$ , and lithological data suggest a detrital source for the clays and hopanes in the intervals of elevated moretane/hopane ratios.

Multiple lines of evidence suggest increased soil erosion, forest fires, continental weathering, and terrigenous input during the PTB (Ward et al., 2000; Retallack et al., 1998; Retallack, 2005; Sephton et al., 2005; Wang and Visscher, 2007; Cao et al., 2009; Nabbefeld et al., 2010b; Shen et al., 2011a,b). Although most studies do not examine evidence earlier than the Changhsingian, detection of particular polycyclic aromatic hydrocarbons (PAHs) in samples from Meishan prior to the extinction horizon suggests that there may have been earlier pulses of land-derived organic matter to the marine system (Nabbefeld et al., 2010b). Interestingly, the highest values of retene, a PAH thought to be derived from coniferous resin (Peters et al., 2005), is concurrent with the earliest interval of moretane/hopane enrichment in the Lungtan Formation. Accordingly, there may have been increased terrigenous input to the marine system during the PTB and the Wuchiapingian, which is consistent with a detrital origin of clays and hopanes during these intervals.

Increased organic matter input from higher plant matter cannot explain the parallel patterns of  $\beta\alpha/(\alpha\beta + \beta\alpha)$  for  $\text{C}_{30-34}$  homohopanes and  $\text{C}_{31-33}$  methylhomohopanes, but increased input of hopanoids from soil bacteria may explain the anomalous moretane/hopane ratios observed in all hopane series. The hypothesis that there was an influx of hopanoids from soil bacteria to the marine system is supported by the observation that high moretane/hopane ratios for all hopane series are associated with high hopane/sterane percentages. This hypothesis is further supported by the observation that high hopane/sterane percentages are associated with high percentages of total clay and high abundances of the clay types that are most tightly related to moretane/hopane ratios (chlorite, illite, mixed layer illite/smectite, and smectite). We conclude that the multiple intervals of elevated moretanes were characterized by increased input of hopanoids derived from soils. However, this change in source input alone does not fully explain the moretane stereochemical anomalies. While  $\beta\alpha$ -hopanoids have been identified in one type of soil bacteria (Rosa-Putra et al., 2001), it is more likely that the detrital clays and redox conditions of the original depositional environment controlled the stereochemistry of the soil-derived hopanoids that were ultimately deposited in marine sediments. Therefore, a combination of hopanoid input from soils and diagenetic effects generated the unique moretane/hopanes patterns observed at Meishan.

#### 4.2. Discussion of possible mechanisms for mineral preservation of $\beta\alpha$ -hopanoid stereochemistry

Certain minerals are known to mediate diagenetic reactions. In addition to thermal maturity and the source of organic matter, depositional environment and lithology are known to affect the distribution of biomarkers, including the moretane/hopane ratio (Moldowan et al., 1986; Curiale and Odermatt, 1989; Peters et al., 2005). If given sufficient time and heat, the biological isomers decline relative to the thermodynamically preferred isomers. However, this simplistic view is further complicated by factors that affect the relative rates of hydrocarbon generation, isomerization,

and thermal degradation (Lu et al., 1989; Farrimond et al., 1998). Mineral composition has been shown to affect the degree of isomerization for steranes and hopanes in natural systems as well as laboratory pyrolysis experiments (Rullkötter et al., 1985; Eglinton et al., 1986; Curiale and Odermatt, 1989; Lu et al., 1989; Peters et al., 1990; Farrimond et al., 1998; Pan et al., 2010), but distinguishing between mineral effects on biomarker genesis, isomerization, and thermal degradation is difficult. Moreover, it is possible that a combination of these mineral composition effects plays a role in controlling biomarker stereoisomer distribution.

Originally, it was believed that the biologically preferred  $\beta\beta$ -hopane was converted to the  $\beta\alpha$ -hopane and  $\alpha\beta$ -hopane according to the energy diagram and schematic depicted in Seifert and Moldowan (1980). The thermodynamic stabilities of the hopane stereoisomers were later confirmed by molecular mechanics (Kolaczowska et al., 1990). However, it was recognized that minerals could modulate the rates of epimerization. In particular, acidic surface sites of certain clay types were shown to catalyze isomerization, rearrangement, and hydrogen exchange reactions (Solomon and Swift, 1967; Sieskind et al., 1979; Saxby et al., 1992). Alexander et al. (1984) proposed an epimerization mechanism that proceeded through a planar  $sp^2$  hybridized intermediate. Due to the enhanced stabilities of tertiary, allylic, or benzylic carbocation and radical intermediates, these positions interact with clay surface sites. The carbon adjacent to the carbocation or radical intermediate then undergoes hydrogen exchange and loss of the original stereochemistry if the hydrogen is added from the opposite face (Alexander et al., 1984). If the mechanism proposed by Alexander et al. (1984) is correct, clay-catalyzed epimerization may be stereoselective. In which case, the conversion of  $\beta\beta$ -hopane to  $\alpha\beta$ -hopane would be less favorable than the conversion to  $\beta\alpha$ -hopane because  $C_{22}$  is arguably the most accessible tertiary carbon in the hopane skeleton that could interact with the clay surface and form a carbocation intermediate, thus promoting epimerization at the adjacent C-21.

However, direct epimerization of the free  $\beta\beta$ -hopane to  $\beta\alpha$ -hopane and  $\alpha\beta$ -hopane isomers is not the only factor that affects the isomeric distribution of hopanes. Indeed, the rates of hydrocarbon release from kerogen and asphaltene, rates of generation of hydrocarbons from functionalized moieties, and rates of hydrocarbon thermal degradation may also play significant roles in controlling isomer distributions of biomarkers. Mineralogy may mediate these processes, thus influencing the initial and final biomarker distribution (Eglinton et al., 1986; Huizinga et al., 1987; Larcher et al., 1988; Lu et al., 1989; Abbott et al., 1990; Bishop and Abbott, 1993; Bishop et al., 1998; Farrimond et al., 1998, 2002; Koopmans et al., 1998; Wei et al., 2006; Pan et al., 2009, 2010). Furthermore, both organic and inorganic protective matrices can affect lipid biomarker distributions (Hedges and Keil, 1995; Huang et al., 2008; Mead and Goni, 2008). Active clay surfaces, in particular, tend to selectively adsorb polar compounds (Pan et al., 2005). For this reason, the preservation and generation mechanisms of polar hopane precursor compounds may offer insight to the moretane anomalies at Meishan detailed in this report.

Hopanoic acids can be a significant source of free hopanes (Bennett and Abbott, 1999). Laboratory and field results have demonstrated that the degree of isomerization of free hopanes is greater than kerogen-bound and functionalized hopanoids, including hopanoic acids (Tannenbaum et al., 1986; Peters and Moldowan, 1991; Bishop et al., 1998; Murray et al., 1998; Farrimond et al., 2002; Lockhart et al., 2008). Isomerization in the hopane E-ring may occur during the decarboxylation of hopanoic acids to yield free hopanes or during bond cleavage of kerogen-bound hopanoids (Farrimond et al., 1998, 2002). Alternatively, rates of isomerization may be slower for bound hopanoids and functionalized hopanoids than for free hopanes, as discussed below.

Hopanoic acids released from kerogen or produced during early diagenesis may become adsorbed on the mineral matrix and/or polar organic matter by ionic interactions (Huizinga et al., 1987; Thomas et al., 1993; Kubicki et al., 1999). Previous works show that “trapped” or “bound” hydrocarbons isomerize at slower rates than free hydrocarbons (Derenne et al., 1988; Jaffé and Gardinali, 1990; Jaffé et al., 1997). Likewise, adsorption of polar moretane precursors to the surface of a protective matrix could effectively retard the rates of isomerization until release at high maturities. Carboxylic acids tend to adsorb strongly on inorganic surfaces (Thomas et al., 1993). However, the preservation potential of the less mature hopanoic acid signature depends on the adsorptive capacity of the mineral surface (Ransom et al., 1998; Kubicki et al., 1999). The different surface chemistries associated with individual clay types have unique affinities for organic matter, which could explain the different correlation strengths observed for  $\beta\alpha/(\alpha\beta + \beta\alpha)$  and the different clay types at Meishan. However, a more comprehensive study is required that characterizes the interaction of polar precursors of hopanoids with the clay types at Meishan and monitors hopanoic acid interactions with the mineral surface over a range of temperature and times.

#### 4.3. Discussion of depositional environment, source input, and $Ts/(Ts+Tm)$

Like the moretane/hopane ratios, the  $Ts/(Ts + Tm)$  thermal maturity parameter is also strongly influenced by source input, lithology, oxicity, and acidity of depositional environment (McKirdy et al., 1983; Moldowan et al., 1986; Waples and Machihara, 1990; Dahl et al., 1993; Peters et al., 2005; Bennett and Olsen, 2007). According to molecular mechanics and observation, Tm (or  $C_{27}$   $17\alpha$ -trisorhopane) is less stable than the rearranged Ts isomer (or  $C_{27}$   $18\alpha$ -trisorhopane) (Seifert and Moldowan, 1978; Kolaczowska et al., 1990). According to Fig. 6,  $Ts/(Ts + Tm)$  seems to be related not only to  $C_{30}$   $\beta\alpha/(\alpha\beta + \beta\alpha)$  as shown in Cao et al. (2009), but it is also inversely related to the  $\beta\alpha/(\alpha\beta + \beta\alpha)$  values of the homohopane and  $2\alpha$ - and  $3\beta$ -methylhomohopane series. This inverse relationship would be expected for  $Ts/(Ts + Tm)$  and  $\beta\alpha/(\alpha\beta + \beta\alpha)$  if thermal maturity was the primary control on these parameters. Like  $\beta\alpha/(\alpha\beta + \beta\alpha)$ ,  $Ts/(Ts + Tm)$  co-varies with total clay percent, specific clay type abundances,  $C_{35}$  HHI, and

hopane/sterane percentages at the Meishan section. As discussed above, maturity parameters that more appropriately evaluate the thermal history of this section, indicate relatively constant thermal maturity through the section, so the same mechanisms that are influencing the moretane/hopane ratios are likely affecting Ts/(Ts + Tm). Unlike previous studies that show that carbonate source rocks tend to generate oil with lower Ts/(Ts + Tm) values than clay-rich source rocks (McKirby et al., 1983; Waples and Machihara, 1990; Peters et al., 2005; Bennett and Olsen, 2007), our results show that low values of Ts/(Ts + Tm) coincide with intervals of high clay content. However, our results are consistent with previous work that indicates Tm is favored over the rearranged, more stable isomer Ts in oxidizing conditions (Moldowan et al., 1986). Like our results that show high values of Ts/(Ts + Tm) in carbonate-rich rocks deposited under reducing conditions, Rullkötter and Marzi (1988) found higher values of Ts/(Ts + Tm) associated with the relatively carbonate-rich Lias  $\epsilon$  unit which was deposited under reducing conditions compared to the adjacent carbonate-poor mudstone facies that was deposited under oxic conditions. Input of soil-derived hopanoids seems to play a role in the moretane/hopane ratio patterns, and the relationship of Ts/(Ts + Tm) with hopane/sterane percentages suggests that source input may be affecting Ts/(Ts + Tm) as well. In total, these results indicate that a combination of source input effects and depositional factors, including oxicity and lithology, control Ts/(Ts + Tm) and complicate the interpretation of this geochemical indicator.

#### 4.4. Discussion of lithology, C<sub>35</sub> homohopane index and additional molecular parameters

Lithology and redox conditions affect other molecular maturity parameters in addition to moretane/hopane ratios and Ts/(Ts + Tm) (Peters et al., 2005). Molecular parameters from Cao et al. (2009), including 28,30-bisnorhopane/C<sub>30</sub> hopane, gammacerane/C<sub>30</sub> hopane, C<sub>29</sub> diasterane/regular sterane, and C<sub>27</sub> diasterane/regular sterane were plotted against percent carbonate, percent total clay, percent total clay/TOC, C<sub>35</sub> HHI, and hopane/sterane percentages. No significant correlations were identified with the exception of an inverse correlation of C<sub>29</sub> diasterane/regular sterane and C<sub>27</sub> diasterane/regular sterane with hopane/sterane percentages. The absence of any relationship with clay/TOC is counter to the results of van Kaam-Peters et al. (1998) and Nabbefeld et al. (2010a), although the different environmental settings, lithologies, and methods may partially explain the discrepancy.

Having recognized a detrital, clay-borne contribution to the hopanoid inventory during intervals of enhanced moretane accumulation at Meishan, the absence of a relationship between diasterane/regular sterane ratio and lithology comes into focus. Terrigenous organic matter tends to have higher abundances of hopanoids and lower contents of steroids relative to TOC compared to marine organic matter (Peters et al., 2005; Handley et al., 2010; Sáenz et al., 2011). Thus, in marine settings the sources of steroids are mainly marine algae from the water column. During sedi-

mentation in a strongly reducing setting, steroids may be relatively unaffected by diagenetic processes associated with the clays. In other words, in this particular environment steroid and hopanoid diagenetic processes are decoupled to the degree that some fraction of the hopanoids is derived from detrital sources while the sterols are predominantly of local origin.

#### 4.5. Potential sources of berthierine

The discovery of measurable berthierine and evidence of trace berthierine in the Lungtan and Yinkeng Formations, respectively, is an observation with multiple possible environmental implications. Berthierine forms in reducing environments, but low levels of sulfide and bicarbonate are also required because pyrite or siderite formation is favored over berthierine formation in reducing conditions in the presence of sulfide and bicarbonate, respectively (Taylor and Curtis, 1995; Fritz and Toth, 1997; Sheldon and Retallack, 2002). Interestingly, the berthierine-rich samples occur in the only kaolinite-rich interval of the section, and kaolinite is implicated in the formation of berthierine (Sheldon and Retallack, 2002). In contrast, samples from the Yinkeng Formation with evidence of trace berthierine are kaolinite-poor and smectite-rich. Smectite and kaolinite signify different weathering conditions, and as a result, the clay composition of these two intervals indicates that two different soil types are contributing to the sediments.

The detection of berthierine in samples from the Lungtan Formation where low C<sub>35</sub> HHI values indicates oxic conditions suggests that one or both of these redox indicators have a detrital component. While it is not possible to conclusively determine from our results whether the berthierine is authigenic or detrital, it is interesting to note that berthierine was discovered in high latitude paleosols deposited in the Early Triassic following the PTB (Sheldon and Retallack, 2002). Formation of berthierine in soils is rare because of the environmental requirements for formation, but weathering or erosion of berthierine-containing paleosols could contribute detrital berthierine to marine sediments. The berthierine-containing paleosols reported in Sheldon and Retallack, 2002 do not correspond well spatially or temporally with the berthierine-rich samples in the Lungtan Formation, but the discovery of berthierine in paleosols may offer a possible mechanism for delivery of berthierine to marine sediments in the event that the berthierine is detrital.

## 5. CONCLUSIONS

Three periods of moretane enhancement, two in the Triassic and one in the Permian, are recorded in the core from the Meishan section in southeastern China. These C<sub>30</sub> moretane/hopane excursions are echoed in the homohopanes and 2 $\alpha$ - and 3 $\beta$ -methylhomohopanes. In light of the multiple and parallel moretane 'anomalies' for the homohopane and 2 $\alpha$ - and 3 $\beta$ -methylhomohopane series, enhanced input from higher plant organic matter does not adequately explain the observed hopane isomer patterns at Meishan. Correlation of high moretane/hopane ratios

with low  $C_{35}$  HHI and high hopane/sterane ratios suggest increased input of hopanoids from soils that are influenced by oxic conditions during transport. However, this shift in source input alone cannot explain the hopane stereochemical patterns at Meishan. Based on  $C_{35}$  HHI and mineralogical analyses, we conclude that diagenetic processes related to lithology and redox determine the  $\beta\alpha$ -moretane/ $\alpha\beta$ -hopane distribution for all of the hopane series throughout the cored interval. It seems likely that certain clay types preferentially bind triterpanes having the moretane configuration. Berthierine, a clay that is formed in reducing conditions, was detected in samples from the Lungtan Formation. It is unclear from our results whether the berthierine is authigenic or detrital, but future determination of the origin of berthierine at Meishan may offer additional environmental insight.

Additional molecular parameters were tested for relationships with lithology. Hopane/sterane ratios,  $C_{35}$  HHI, percent total clay, chlorite, illite, and illite/smectite mixed layer clay showed significant relationships with Ts/(Ts + Tm), suggesting source input, lithology, and redox also affect this ratio. However, unlike previous studies (van Kaam-Peters et al., 1998; Nabbefeld et al., 2010a) that reported a link between diasteranes and percent clay/TOC, this relationship was noticeably absent in the sediments at Meishan. Therefore, it seems likely that the diagenesis of steroids here was decoupled from the clay component and more under the control of the intense reducing conditions that prevailed in the water column. In total, our results point toward a complex role of redox and lithology in the transformation of organic matter during diagenesis and maturation. Future work is required to disentangle the lithological effects on diagenetic processes, including biomarker genesis isomerization, and thermal degradation. We conclude that a combination of episodic hopanoid input from soil bacteria and diagenetic effects related to redox and detrital clays generated the distinctive moretane/hopane patterns at Meishan.

#### ACKNOWLEDGMENTS

We wish to thank Christian Hallman and Jürgen Rullkötter for discussions and constructive suggestions, and Gordon Love for his contributions to the early stages of this work, and Bob Burruss, Simon George, and Ken Peters for informative reviews and insightful comments that strengthened this work. K.L.F. is supported by a National Science Foundation Graduate Research Fellowship. Research at MIT was supported by an award (NNX09AM88G) from the NASA Exobiology Program to R.E.S. Research at Nanjing was supported by the 973 Project of the MST of China (2011CB808905) and NSF of China. N.J.T. acknowledges support from Churchill College and the Royal Society (RG 2009/R<sup>2</sup>).

#### REFERENCES

- Abbott G., Wang G., Eglinton T., Home A. and Petch G. (1990) The kinetics of sterane biological marker release and degradation processes during the hydrous pyrolysis of vitrinite kerogen. *Geochim. Cosmochim. Acta* **54**, 2451–2461.
- Aichner B., Wilkes H., Herzschuh U., Mischke S. and Zhang C. (2010) Biomarker and compound-specific  $\delta^{13}C$  evidence for changing environmental conditions and carbon limitation at Lake Koucha, eastern Tibetan Plateau. *J. Paleolimnol.* **43**, 873–899.
- Alexander R., Kagi R. and Larcher A. (1984) Clay catalysis of alkyl hydrogen exchange reactions—reaction mechanisms. *Org. Geochem.* **6**, 755–760.
- Barnosky A. D., Matzke N., Tomiya S., Wogan G. O. U., Swartz B., Quental T. B., Marshall C., Mcguire J. L., Lindsey E. L., Maguire K. C., Mersey B. and Ferrer E. A. (2011) Has the Earth's sixth mass extinction already arrived?. *Nature* **470** 51–57.
- Bauer P., Dunlap N., Arseniyadis S., Watt D., Seifert W. and Moldovan J. (1983) Synthesis of biological markers in fossil fuels. 1.  $17\alpha$  and  $17\beta$  isomers of 30-norhopane and 30-normoretane. *J. Org. Chem.* **48**, 4493–4497.
- Becker L., Poreda R., Hunt A., Bunch T. and Rampino M. (2001) Impact event at the Permian–Triassic boundary: evidence from extraterrestrial noble gases in fullerenes. *Science* **291**, 1530–1533.
- Bennett B. and Abbott G. (1999) A natural pyrolysis experiment – hopanes from hopanoic acids? *Org. Geochem.* **30**, 1509–1516.
- Bennett B. and Olsen S. D. (2007) The influence of source depositional conditions on the hydrocarbon and nitrogen compounds in petroleum from central Montana, USA. *Org. Geochem.* **38**, 935–956.
- Benton M. and Twitchett R. (2003) How to kill (almost) all life: the end-Permian extinction event. *Trends Ecol. Evol.* **18**, 358–365.
- Bishop A. and Abbott G. (1993) The interrelationship of biological marker maturity parameters and molecular yields during contact-metamorphism. *Geochim. Cosmochim. Acta* **57**, 3661–3668.
- Bishop A., Love G., McAulay A., Snape C. and Farrimond P. (1998) Release of kerogen-bound hopanoids by hydrolysis. *Org. Geochem.* **29**, 989–1001.
- Campbell I., Czamanske G., Fedorenko V., Hill R. and Stepanov V. (1992) Synchronism of the Siberian traps and the Permian–Triassic boundary. *Science* **258**, 1760–1763.
- Cao C., Love G. D., Hays L., Wang W., Shen S. and Summons R. E. (2009) Biogeochemical evidence for euxinic oceans and ecological disturbance presaging the end-Permian mass extinction event. *Earth Planet. Sci. Lett.* **281**, 188–201.
- Cao C., Wang W. and Jin Y. (2002) Carbon isotope excursions across the Permian–Triassic boundary in the Meishan section, Zhejiang Province, China. *Chinese Sci. Bull.* **47**, 1125–1129.
- Curiale J. and Odermatt J. (1989) Short-term biomarker variability in the Monterey Formation, Santa Maria Basin. *Org. Geochem.* **14**, 1–13.
- Dahl J., Michael Moldovan J. and Sundararaman P. (1993) Relationship of biomarker distribution to depositional environment: phosphoria Formation, Montana, USA. *Org. Geochem.* **20**, 1001–1017.
- Derenne S., Largeau C., Casadevall E. and Connan J. (1988) Comparison of torbanites of various origins and evolutionary stages. Bacterial contribution to their formation. Causes of the lack of botryococcane in bitumens. *Org. Geochem.* **12**, 43–59.
- Eglinton T., Rowland S., Curtis C. and Douglas A. (1986) Kerogen–mineral reactions at raised temperatures in the presence of water. *Org. Geochem.* **10**, 1041–1052.
- Erwin D. H. (2006) *Extinction: how life on earth nearly ended 250 million years ago*. Princeton University Press, Princeton, NJ, USA.
- Farrimond P., Griffiths T. and Evdokiadis E. (2002) Hopanoic acids in Mesozoic sedimentary rocks: their origin and relationship with hopanes. *Org. Geochem.* **33**, 965–977.
- Farrimond P., Taylor A. and Telnaes N. (1998) Biomarker maturity parameters: the role of generation and thermal degradation. *Org. Geochem.* **29**, 1181–1197.

- Fritz S. and Toth T. (1997) An Fe-berthierine from a Cretaceous laterite. 2. Estimation of Eh, pH and pCO<sub>2</sub> conditions of formation. *Clay Clay Mineral.* **45**, 580–586.
- Grantham P. (1986) Sterane isomerisation and moretane/hopane ratios in crude oils derived from Tertiary source rocks. *Org. Geochem.* **9**, 293–304.
- Grice K., Cao C., Love G., Bottcher M., Twitchett R., Grosjean E., Summons R., Turgeon S., Dunning W. and Jin Y. (2005) Photic zone euxinia during the Permian–Triassic superanoxic event. *Science* **307**, 706–709.
- Handley L., Talbot H., Cooke M., Anderson K. and Wagner T. (2010) Bacterioplanepolyols as tracers for continental and marine organic matter supply and phases of enhanced nitrogen cycling on the late Quaternary Congo deep sea fan. *Org. Geochem.* **41**, 910–914.
- Hedges J. I. and Keil R. G. (1995) Sedimentary organic matter preservation: an assessment and speculative synthesis. *Mar. Chem.* **49**, 81–115.
- Huang X., Cui J., Pu Y., Huang J. and Blyth A. J. (2008) Identifying “free” and “bound” lipid fractions in stalagmite samples: an example from Heshang Cave, Southern China. *Appl. Geochem.* **23**, 2589–2595.
- Hughes W. B. and Dzou L. I. P. (1995) Reservoir overprinting of crude oils. *Org. Geochem.* **23**, 905–914.
- Huizinga B., Tannenbaum E. and Kaplan I. (1987) The role of minerals in the thermal alteration of organic-matter. 4. Generation of normal-alkanes, acyclic isoprenoids, and alkenes in laboratory experiments. *Geochim. Cosmochim. Acta* **51**, 1083–1097.
- Hveding-Bergseth N., Bruun T. and Kjusen H. (1983) Isolation of 30-nor-21 [alpha]-hopan-22-one (isoadiantone) from the lichen *Platismatia glauca*. *Phytochemistry* **22**, 1826–1827.
- Isaksen G. and Bohacs K. (1995) Geologic controls of source rock geochemistry through relative sea level. In *Petroleum Source Rocks* (ed. B. Katz). Springer-Verlag, Berlin, New York, pp. 25–50.
- Ishiwatari R., Yamamoto S. and Uemura H. (2005) Lipid and lignin/cutin compounds in Lake Baikal sediments over the last 37 kyr: implications for glacial-interglacial palaeoenvironmental change. *Org. Geochem.* **36**, 327–347.
- Jaffé R., Diaz D., Hajje N., Chen L., Eckardt C. and Furton K. G. (1997) Hydrocarbon speciation in ancient sediments studied by stepwise high-temperature supercritical carbon dioxide extraction. *Org. Geochem.* **26**, 59–65.
- Jaffé R. and Gardinali P. (1990) Generation and maturation of carboxylic acids in ancient sediments from the Maracaibo Basin, Venezuela. *Org. Geochem.* **16**, 211–218.
- Kaiho K., Chen Z.-Q., Kawahata H., Kajiwaru Y. and Sato H. (2006) Close-up of the end-Permian mass extinction horizon recorded in the Meishan section, South China: sedimentary, elemental, and biotic characterization and a negative shift of sulfate sulfur isotope ratio. *Palaeogeogr. Palaeoclimatol. Palaeoecol.* **239**, 396–405.
- Kaiho K., Kajiwaru Y., Nakano T., Miura Y., Kawahata H., Tazaki K., Ueshima M., Chen Z. and Shi G. (2001) End-Permian catastrophe by a bolide impact: evidence of a gigantic release of sulfur from the mantle. *Geology* **29**, 815–818.
- Kamo S., Czamanske G., Amelin Y., Fedorenko V., Davis D. and Trofimov V. (2003) Rapid eruption of Siberian flood-volcanic rocks and evidence for coincidence with the Permian–Triassic boundary and mass extinction at 251 Ma. *Earth Planet. Sci. Lett.* **214**, 75–91.
- Kolaczowska E., Slougui N., Watt D., Maruca R. and Michael Moldowan J. (1990) Thermodynamic stability of various alkylated, dealkylated and rearranged 17 $\alpha$ - and 17 $\beta$ -hopane isomers using molecular mechanics calculations. *Org. Geochem.* **16**, 1033–1038.
- Koopmans M., Carson F., Sinninghe Damsté J. and Lewan M. (1998) Biomarker generation from Type II-S kerogens in claystone and limestone during hydrous and anhydrous pyrolysis. *Org. Geochem.* **29**, 1395–1402.
- Kristen I., Wilkes H., Vieth A., Zink K.-G., Plessen B., Thorpe J., Partridge T. C. and Oberhaensli H. (2010) Biomarker and stable carbon isotope analyses of sedimentary organic matter from Lake Tswaing: evidence for deglacial wetness and early Holocene drought from South Africa. *J. Paleolimnol.* **44**, 143–160.
- Kubicki J., Schroeter L., Itoh M., Nguyen B. and Apitz S. (1999) Attenuated total reflectance Fourier-transform infrared spectroscopy of carboxylic acids adsorbed onto mineral surfaces. *Geochim. Cosmochim. Acta* **63**, 2709–2725.
- Larcher A., Alexander R. and Kagi R. (1987) Changes in configuration of extended moretanes with increasing sediment maturity. *Org. Geochem.* **11**, 59–63.
- Larcher A., Alexander R. and Kagi R. (1988) Differences in reactivities of sedimentary hopane diastereomers when heated in the presence of clays. *Org. Geochem.* **13**, 665–669.
- Lavie D., Jain T. and Mahendra K. (1968) Terpenoids–VII. Constituents of *Euphorbia lateriflora* Schum and Thonn. *Phytochemistry* **7**, 657–660.
- Lockhart R. S., Meredith W., Love G. D. and Snape C. E. (2008) Release of bound aliphatic biomarkers via hydrolysis from Type II kerogen at high maturity. *Org. Geochem.* **39**, 1119–1124.
- Looy C., Twitchett R., Dilcher D., Konijnenburg-Van Cittert J. and Visscher H. (2001) Life in the end-Permian dead zone. *Proc. Natl. Acad. Sci. USA* **98**, 7879–7883.
- Lu S., Ruth E. and Kaplan I. (1989) Pyrolysis of kerogens in the absence and presence of montmorillonite- I. The generation, degradation and isomerization of steranes and triterpanes at 200-Degrees-C and 300-Degrees-C. *Org. Geochem.* **14**, 491–499.
- McKirdy D., Aldridge A. and Ypma P. (1983) A geochemical comparison of some crude oils from Pre-Ordovician carbonate rocks. In *Adv. Org. Geochem.* (ed. M. Bjoroy). John Wiley and Sons, New York, pp. 99–107.
- Mead R. N. and Goni M. A. (2008) Matrix protected organic matter in a river dominated margin: a possible mechanism to sequester terrestrial organic matter? *Geochim. Cosmochim. Acta* **72**, 2673–2686.
- Metcalfe I. and Isozaki Y. (2009) Current perspectives on the Permian–Triassic boundary and end-Permian mass extinction: preface. *J. Asian Earth Sci.* **36**, 407–412.
- Michaelsen P. (2002) Mass extinction of peat-forming plants and the effect on fluvial styles across the Permian–Triassic boundary, northern Bowen Basin, Australia. *Palaeogeogr. Palaeoclimatol. Palaeoecol.* **179**, 173–188.
- Moldowan J., Sundararaman P. and Schoell M. (1986) Sensitivity of biomarker properties to depositional environment and/or source input in the Lower Toarcian of SW-Germany. *Org. Geochem.* **10**, 915–926.
- Mundil R., Ludwig K., Metcalfe I. and Renne P. (2004) Age and timing of the Permian mass extinctions: U/Pb dating of closed-system zircons. *Science* **305**, 1760–1763.
- Mundil R., Metcalfe I., Ludwig K. R., Renne P. R., Oberli F. and Nicoll R. S. (2001) Timing of the Permian–Triassic biotic crisis: implications from new zircon U/Pb age data (and their limitations). *Earth Planet. Sci. Lett.* **187**, 131–145.
- Murray I., Love G., Snape C. and Bailey N. (1998) Comparison of covalently-bound aliphatic biomarkers released via hydrolysis with their solvent-extractable counterparts for a suite of Kimmeridge clays. *Org. Geochem.* **29**, 1487–1505.

- Nabbefeld B., Grice K., Schimmelmann A., Summons R. E., Troitzsch U. and Twitchett R. J. (2010a) A comparison of thermal maturity parameters between freely extracted hydrocarbons (Bitumen I) and a second extract (Bitumen II) from within the kerogen matrix of Permian and Triassic sedimentary rocks. *Org. Geochem.* **41**, 78–87.
- Nabbefeld B., Grice K., Summons R. E., Hays L. E. and Cao C. (2010b) Significance of polycyclic aromatic hydrocarbons (PAHs) in Permian/Triassic boundary sections. *Appl. Geochem.* **25**, 1374–1382.
- Ouirsson G. and Albrecht P. (1992) Hopanoids. I. Geohopanoids – the most abundant natural-products on earth. *Acc. Chem. Res.* **25**, 398–402.
- Pan C., Feng J., Tian Y., Yu L., Luo X., Sheng G. and Fu J. (2005) Interaction of oil components and clay minerals in reservoir sandstones. *Org. Geochem.* **36**, 633–654.
- Pan C., Geng A., Zhong N. and Liu J. (2010) Kerogen pyrolysis in the presence and absence of water and minerals: steranes and triterpenoids. *Fuel* **89**, 336–345.
- Pan C., Geng A., Zhong N., Liu J. and Yu L. (2009) Kerogen pyrolysis in the presence and absence of water and minerals: amounts and compositions of bitumen and liquid hydrocarbons. *Fuel* **88**, 909–919.
- Peters K. and Moldowan J. (1991) Effects of source, thermal maturity, and biodegradation on the distribution and isomerization of homohopanes in petroleum. *Org. Geochem.* **17**, 47–61.
- Peters K., Moldowan J. and Sundararaman P. (1990) Effects of hydrous pyrolysis on biomarker thermal maturity parameters: monterey phosphatic and siliceous members. *Org. Geochem.* **15**, 249–265.
- Peters K. E., Walters C. C. and Moldowan J. M. (2005) *The Biomarker Guide*, 2nd ed. Cambridge University Press, Cambridge, UK, New York.
- Pollastro R. M. (1993) Considerations and applications of the illite/smectite geothermometer in hydrocarbon-bearing rocks of Miocene to Mississippian age. *Clay Clay Mineral.* **41**, 119–133.
- Quirk M., Wardroper A., Wheatley R. and Maxwell J. (1984) Extended hopanoids in peat environments. *Chem. Geol.* **42**, 25–43.
- Ransom B., Kim D., Kastner M. and Wainwright S. (1998) Organic matter preservation on continental slopes: importance of mineralogy and surface area. *Geochim. Cosmochim. Acta* **62**, 1329–1345.
- Raup D. (1979) Size of the Permo–Triassic bottleneck and its evolutionary implications. *Science* **206**, 217–218.
- Renne P., Black M., Zichao Z., Richards M. and Basu A. (1995) Synchrony and causal relations between Permian–Triassic boundary crises and Siberian flood volcanism. *Science* **269**, 1413–1416.
- Retallack G. (1995) Permian–Triassic life crisis on land. *Science* **267**, 77–80.
- Retallack G., Seyedolali A., Krull E., Holser W., Ambers C. and Kyte F. (1998) Search for evidence of impact at the Permian–Triassic boundary in Antarctica and Australia. *Geology* **26**, 979–982.
- Retallack G. (2005) Earliest Triassic claystone breccias and soil-erosion crisis. *J. Sed. Res.* **75**, 679–695.
- Reynolds, Jr., R. C. and Reynolds, III, R. C. (1996) *NEWMOD for windows: the calculation of one dimensional X-ray diffraction patterns of mixed-layered clay minerals*. Computer program, R.C. Reynolds, Hanover, NH, USA.
- Rosa-Putra S., Nalin R., Domenach A. and Rohmer M. (2001) Novel hopanoids from *Frankia* spp. and related soil bacteria. *Eur. J. Biochem.* **268**, 4300–4306.
- Rullkötter J. and Marzi R. (1988) Natural and artificial maturation of biological markers in a Toarcian shale from northern Germany. *Org. Geochem.* **13**, 639–645.
- Rullkötter J., Spiro B. and Nissenbaum A. (1985) Biological marker characteristics of oils and asphalts from carbonate source rocks in a rapidly subsiding graben, Dead Sea, Israel. *Geochim. Cosmochim. Acta* **49**, 1357–1370.
- Sáenz J., Eglinton T. and Summons R. (2011) Abundance and structural diversity of bacteriohopanepolyols in suspended particulate matter along a river ocean transect. *Org. Geochem.* **42**, 774–780.
- Saxby J., Chatfield P., Taylor G., Fitzgerald J., Kaplan I. and Lu S. (1992) Effect of clay minerals on products from coal maturation. *Org. Geochem.* **18**, 373–383.
- Seifert W. and Moldowan J. (1980) The effect of thermal stress on source-rock quality as measured by hopane stereochemistry. *Phys. Chem. Earth* **12**, 229–237.
- Seifert W. and Moldowan M. (1978) Applications of steranes, terpanes and monoaromatics to the maturation, migration and source of crude oils. *Geochim. Cosmochim. Acta* **42**, 77–95.
- Sephton M. A., Looy C. V., Brinkhuis H., Wignall P. B., De Leeuw J. W. and Visscher H. (2005) Catastrophic soil erosion during the end-Permian biotic crisis. *Geology* **33**, 941–944.
- Sepkoski J. J. (2002) A compendium of fossil marine animal genera. *Bull. Am. Paleontol.* **363**, 1–563.
- Sheldon N. D. and Retallack G. J. (2002) Low oxygen levels in earliest Triassic. *Geology* **30**, 919–922.
- Shen J. and Huang W. (2007) Biomarker distributions as maturity indicators in coals, coaly shales, and shales from Taiwan. *Terr. Atmos. Ocean Sci.* **18**, 739–755.
- Shen S., Crowley J., Wang Y., Bowring S., Erwin D., Sadler P., Cao C., Rothman D., Henderson C., Ramezani J., Zhang H., Shen Y., Wang X., Wang W., Mu L., Li W., Tang Y., Liu X., Liu L., Zeng Y., Jiang Y. and Jin Y. (2011a) Calibrating the end-Permian mass extinction. *Science* **17** (10.1126/science.1213454).
- Shen W., Sun Y., Lin Y., Liu D. and Chai P. (2011b) Evidence of wildfire in the Meishan section and implications for Permian–Triassic events. *Geochim. Cosmochim. Acta* **75**, 1992–2006.
- Shiojima K. and Ageta H. (1990) Fern constituents: two new triterpenoid hydrocarbons, hop-16-ene and isohop-22(29)-ene, isolated from *Davallia-mariësii*. *Chem. Pharm. Bull.* **38**, 347–349.
- Sieskind O., Joly G. and Albrecht P. (1979) Simulation of the geochemical transformations of sterols – superacid effect of clay–minerals. *Geochim. Cosmochim. Acta* **43**, 1675–1679.
- Solomon D. and Swift J. (1967) Reactions catalyzed by minerals. Part II. chain termination in free-radical polymerizations. *J. Appl. Polym. Sci.* **11**, 2567–2575.
- Srodon J., Drits V., McCarty D., Hsieh J. and Eberl D. (2001) Quantitative X-ray diffraction analysis of clay-bearing rocks from random preparations. *Clay Clay Mineral.* **49**, 514–528.
- Tannenbaum E., Ruth E. and Kaplan I. (1986) Steranes and triterpanes generated from kerogen pyrolysis in the absence and presence of minerals. *Geochim. Cosmochim. Acta* **50**, 805–812.
- Taylor K. and Curtis C. (1995) Stability and facies association of early diagenetic mineral assemblages; an example from a Jurassic ironstone-mudstone succession, UK. *J. Sediment Res.* **A65**, 358–368.
- Thomas M., Clouse J. and Longo J. (1993) Adsorption of organic compounds on carbonate minerals. 1. Model compounds and their influence on mineral wettability. *Chem. Geol.* **109**, 201–213.
- Tsuzuki K., Ohashi A., Arai Y., Masuda K., Takano A., Shiojima K., Ageta H. and Cai S. (2001) Triterpenoids from *Adiantum caudatum*. *Phytochemistry* **58**, 363–367.

- Twitchett R., Looy C., Morante R., Visscher H. and Wignall P. (2001) Rapid and synchronous collapse of marine and terrestrial ecosystems during the end-Permian biotic crisis. *Geology* **29**, 351–354.
- Uemura H. and Ishiwatari R. (1995) Identification of unusual 17 [beta](H)-moret-22 (29)-ene in lake sediments. *Org. Geochem.* **23**, 675–680.
- van Kaam-Peters H. M. E., Köster J., van der Gaast S. J., Dekker M., de Leeuw J. W. and Sinninghe Damsté J. S. (1998) The effect of clay minerals on diasterane/sterane ratios. *Geochim. Cosmochim. Acta* **62**, 2923–2929.
- Wang C. (2007) Anomalous hopane distributions at the Permian–Triassic boundary, Meishan, China—Evidence for the end-Permian marine ecosystem collapse. *Org. Geochem.* **38**, 52–66.
- Wang C. and Visscher H. (2007) Abundance anomalies of aromatic biomarkers in the Permian–Triassic boundary section at Meishan, China – evidence of end-Permian terrestrial ecosystem collapse. *Palaeogeogr. Palaeoclimatol. Palaeoecol.* **252**, 291–303.
- Wang C., Liu Y., Liu H., Zhu L. and Shi Q. (2005) Geochemical significance of the relative enrichment of pristane and the negative excursion of delta C-13(Pr) across the Permian–Triassic Boundary at Meishan, China. *Chinese Sci. Bull.* **50**, 2213–2225.
- Waples D. and Machihara T. (1990) Applications of sterane and triterpane biomarkers in petroleum exploration. *Bull. Can. Petrol. Geol.* **38**, 357–380.
- Ward P. D., Montgomery D. R. and Smith R. (2000). *Altered river morphology in South Africa related to the Permian–Triassic Extinction* **289**, 1740–1743.
- Wei Z., Moldowan J. and Paytan A. (2006) Diamondoids and molecular biomarkers generated from modern sediments in the absence and presence of minerals during hydrous pyrolysis. *Org. Geochem.* **37**, 891–911.
- Wignall P. and Hallam A. (1992) Anoxia as a cause of the Permian/Triassic mass extinction: facies evidence from northern Italy and the western United States. *Palaeogeogr. Palaeoclimatol. Palaeoecol.* **93**, 21–46.
- Xie S., Pancost R., Huang J., Wignall P., Yu J., Tang X., Chen L., Huang X. and Lai X. (2007) Changes in the global carbon cycle occurred as two episodes during the Permian–Triassic crisis. *Geology* **35**, 1083–1086.
- Xie S., Pancost R., Yin H., Wang H. and Evershed R. (2005) Two episodes of microbial change coupled with Permo/Triassic faunal mass extinction. *Nature* **434**, 494–497.

Associate editor: Robert C. Burruss